Annu. Rev. Astro. Astrophys. 2006.44:17-47. Downloaded from arjournals.annualreviews.org
by University of Bologna on 10/31/08. For personal use only.

The Evolution and Structure of Pulsar Wind Nebulae

Bryan M. Gaensler[1] and Patrick O. Slane

Harvard-Smithsonian Center for Astrophysics, 60 Garden Street, Cambridge, Massachusetts 02138; email: bgaensler@cfa.harvard.edu, pslane@cfa.harvard.edu

Annu. Rev. Astron. Astrophys. 2006. 44:17–47

First published online as a Review in Advance on April 25, 2006

The *Annual Review of Astrophysics* is online at astro.annualreviews.org

doi: 10.1146/annurev.astro.44.051905.092528

Copyright © 2006 by Annual Reviews. All rights reserved

0066-4146/06/0922-0017$20.00

[1]Current address: School of Physics, University of Sydney, NSW 2006, Australia

Key Words

acceleration of particles, magnetic fields, shock waves, supernova remnants, winds and outflows

Abstract

Pulsars steadily dissipate their rotational energy via relativistic winds. Confinement of these outflows generates luminous pulsar wind nebulae, seen across the electromagnetic spectrum in synchrotron and inverse Compton emission and in optical emission lines when they shock the surrounding medium. These sources act as important probes of relativistic shocks, particle acceleration, and interstellar gas. We review the many recent advances in the study of pulsar wind nebulae, with particular focus on the evolutionary stages through which these objects progress as they expand into their surroundings, and on morphological structures within these nebulae that directly trace the physical processes of particle acceleration and outflow. We conclude by considering some exciting new probes of pulsar wind nebulae, including the study of TeV gamma-ray emission from these sources, and observations of pulsar winds in close binary systems.

Annu. Rev. Astro. Astrophys. 2006.44:17-47. Downloaded from arjournals.annualreviews.org
by University of Bologna on 10/31/08. For personal use only.

1. INTRODUCTION

SN(e): supernova(e)

The Crab Nebula (**Figure 1**) is almost certainly associated with a supernova explosion observed in 1054 CE (Stephenson & Green 2002, and references therein). However, this source differs substantially from what is now seen at the sites of other recent SNe, in that the Crab Nebula is centrally filled at all wavelengths, whereas sources such as Tycho's and Kepler's supernova remnants show a shell morphology. This and other simple observations show that the Crab Nebula is anomalous, its energetics dominated by continuous injection of magnetic fields and relativistic particles from a central source.

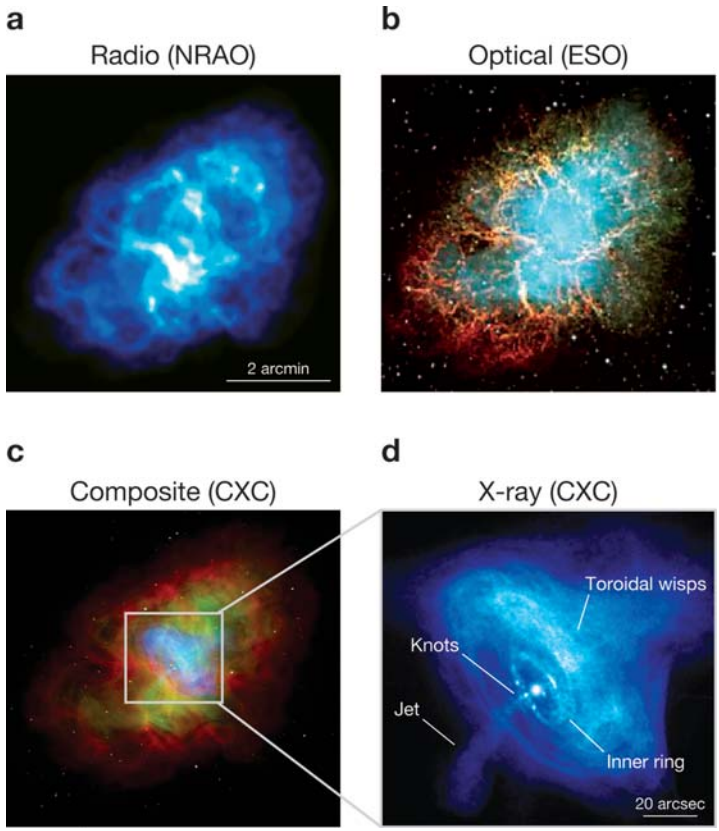

Figure 1

Images of the Crab Nebula (G184.6–5.8). (*a*) Radio synchrotron emission from the confined wind, with enhancements along filaments. (*b*) Optical synchrotron emission (*blue-green*) surrounded by emission lines from filaments (*red*). (*c*) Composite image of radio (*red*), optical (*green*), and X-ray (*blue*) emission. (*d*) X-ray synchrotron emission from jets and wind downstream of the termination shock, marked by the inner ring. Note the decreasing size of the synchrotron nebula going from the radio to the X-ray band. Each image is oriented with north up and east to the left. The scale is indicated by the 2 arcmin scale bar, except for panel (*d*), where the 20 arcsec scale bar applies.

A 16th magnitude star embedded in the Crab Nebula was long presumed to be the stellar remnant and central engine (Minkowski 1942; Pacini 1967). This was confirmed when 33-ms optical and radio pulsations were detected from this star in the late 1960s (Staelin & Reifenstein 1968; Cocke, Disney & Taylor 1969), and these pulsations were then shown to be slowing down at a rate of 36 ns per day (Richards & Comella 1969). The conclusion was quickly reached that the Crab Nebula contains a rapidly rotating young neutron star, or "pulsar," formed in the SN of 1054 CE. The observed rate of spin down implies that kinetic energy is being dissipated at a rate of $\sim 5 \times 10^{38}$ ergs s^{-1}, a value similar to the inferred rate at which energy is being supplied to the nebula (Gold 1969). Following this discovery, a theoretical understanding was soon developed in which the central pulsar generates a magnetized particle wind, whose ultrarelativistic electrons and positrons radiate synchrotron emission across the electromagnetic spectrum (Pacini & Salvati 1973; Rees & Gunn 1974). The pulsar has steadily released about a third of its total reservoir of $\sim 5 \times 10^{49}$ ergs of rotational energy into its surrounding nebula over the last 950 years. This is in sharp contrast to shell-like SNRs, in which the dominant energy source is the $\sim 10^{51}$ ergs of kinetic energy released at the moment of the original SN explosion.

SNR: supernova remnant

Neutron star: a compact degenerate stellar remnant, formed in the core-collapse of a massive star

Pulsar: a rapidly rotating, highly-magnetized neutron star, which generates coherent beams of radiation along its magnetic poles

Pulsar wind nebula(e) [PWN(e)]: a bubble of shocked relativistic particles, produced when a pulsar's relativistic wind interacts with its environment

Observations over the past several decades have identified 40 to 50 further sources, in both our own Galaxy and in the Magellanic Clouds, with properties similar to those of the Crab Nebula (Kaspi, Roberts & Harding 2006; Green 2004)—these sources are known as "pulsar wind nebulae."[1] Sometimes a PWN is surrounded by a shell-like SNR, and the system is termed "composite" (see **Figure 2**). In other cases, best typified by the Crab itself, no surrounding shell is seen.[2]

More recently, an additional category of PWNe has been identified, in which pulsars with high space velocities produce nebulae with cometary or bow shock morphologies as they move through the interstellar medium at supersonic speeds. The sample of such sources is currently small, but high spatial resolution observations, especially in the X-ray band, are rapidly adding to this group.

Because PWNe have a well-defined central energy source and are close enough to be spatially resolved, they act as a marvelous testing ground for studying both relativistic flows and the shocks that result when these winds collide with their surroundings. Studies of PWNe, particularly the spectacular images now being taken by the *Chandra X-ray Observatory*, allow us to resolve details of the interaction of relativistic flows with their surroundings that may never be possible in other classes of source, and can provide the physical foundation for understanding a wide range of astrophysical problems.

We here review current understanding of the structure and evolution of PWNe, with an emphasis on the explosion of new data and new ideas that have emerged in the past few years. Our focus is primarily observational; theoretical considerations

[1] PWNe are also often referred to as "plerions." However, given this term's obscure origin (Weiler & Panagia 1978; Shakeshaft 1979), we avoid using this terminology here.

[2] The absence of a shell around the Crab Nebula is presumably because it has not yet interacted with sufficient surrounding gas (Frail et al., 1995; Seward, Gorenstein & Smith 2006).

Annu. Rev. Astro. Astrophys. 2006.44:17-47. Downloaded from arjournals.annualreviews.org
by University of Bologna on 10/31/08. For personal use only.

Annu. Rev. Astro. Astrophys. 2006.44:17-47. Downloaded from arjournals.annualreviews.org
by University of Bologna on 10/31/08. For personal use only.

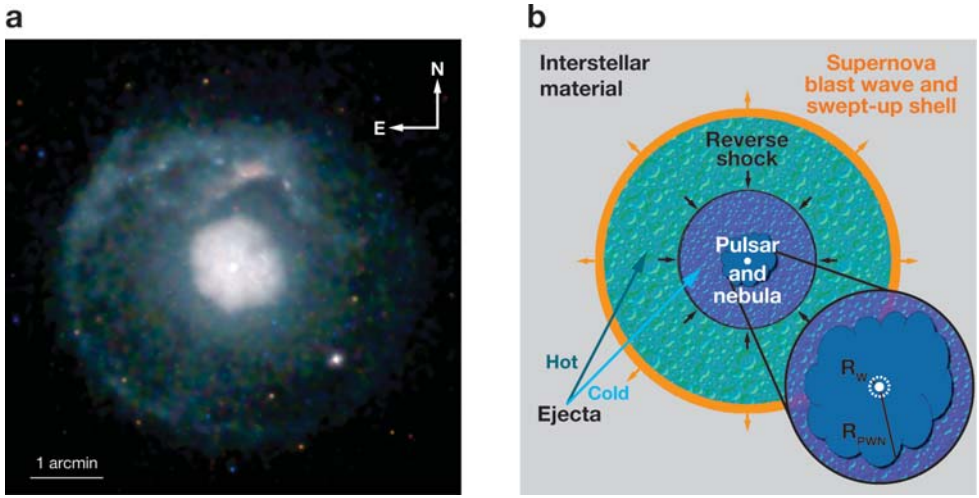

Figure 2

(*a*) A deep *Chandra* X-ray image of the composite SNR G21.5–0.9 (Matheson & Safi-Harb 2005). A circular supernova remnant (SNR) of diameter ≈5′ surrounds a symmetric pulsar wind nebula (PWN) of diameter ≈1.′5, with the young pulsar J1833-1034 at the center (Gutpa et al., 2005; Camilo et al., 2006). The central location of the pulsar and PWN and the symmetric appearance of the PWN and SNR both argue for a relatively unevolved system in which the PWN expands freely and symmetrically into the unshocked interior of the SNR. (*b*) A schematic diagram of a composite SNR showing the swept-up interstellar medium shell, hot and cold ejecta separated by the reverse shock, and the central pulsar and its nebula. The expanded PWN view shows the wind termination shock. Note that this diagram does not correspond directly to G21.5–0.9, in that a significant reverse shock has probably yet to form in this young SNR.

have been recently discussed by van der Swaluw, Downes & Keegan (2004), Melatos (2004), and Chevalier (2005).

The outline of this review is as follows: in Section 2 we explain the basic observational properties of pulsars and their nebulae; in Section 3 we review current understanding of the evolutionary sequence spanned by the observed population of PWNe; in Section 4 we discuss observations of PWNe around young pulsars, which represent the most luminous and most intensively studied component of the population; in Section 5 we consider the properties of the bow shocks produced by high velocity pulsars; and in Section 6 we briefly describe other recent and interesting results in this field.

2. OVERALL PROPERTIES

2.1. Pulsar Spin Down

Because a pulsar's rotational energy, E_{rot}, is the source for most of the emission seen from PWNe, we first consider the spin evolution of young neutron stars.

Annu. Rev. Astro. Astrophys. 2006.44:17-47. Downloaded from arjournals.annualreviews.org
by University of Bologna on 10/31/08. For personal use only.

2.1.1. Spin-down luminosity, age, and magnetic field. An isolated pulsar has a spin period, P, and a period derivative with respect to time, $\dot{P} \equiv dP/dt$, both of which can be determined from observations of the pulsed signal.

The "spin down luminosity" of the pulsar, $\dot{E} = -dE_{rot}/dt$, is the rate at which rotational kinetic energy is dissipated, and is thus given by the equation:

$$\dot{E} \equiv 4\pi^2 I \frac{\dot{P}}{P^3}, \tag{1}$$

where I is the neutron star's moment of inertia, which for a mass of $1.4\,M_\odot$ and a radius of 10 km has the value 10^{45} g cm^{-2}. Values of $\dot{E}$ for the observed pulsar population range between $\approx 5 \times 10^{38}$ ergs s^{-1} for the Crab pulsar and PSR J0537-6910, down to 3×10^{28} ergs s^{-1} for the slowest known pulsar, PSR J2144-3933 (Manchester et al., 2005). Typically only pulsars with $\dot{E} \gtrsim 4 \times 10^{36}$ ergs s^{-1} (of which $\sim$15 are currently known) produce prominent PWNe (Gotthelf 2004).

The age and surface magnetic field strength of a neutron star can be inferred from P and $\dot{P}$, subject to certain assumptions. If a pulsar spins down from an initial spin period P_0 such that $\dot{\Omega} = -k\Omega^n$ (where $\Omega = 2\pi/P$ and n is the "braking index"), then the age of the system is (Manchester & Taylor 1977)

$$\tau = \frac{P}{(n-1)\dot{P}} \left[1 - \left(\frac{P_0}{P} \right)^{n-1} \right], \tag{2}$$

where we have assumed k to be a constant and $n \neq 1$. The braking index, n, has only been confidently measured for four pulsars (Livingstone, Kaspi & Gavriil 2005, and references therein), in each case falling in the range $2 < n < 3$.

If for the rest of the population we assume $n = 3$ (corresponding to spin down via magnetic dipole radiation) and $P_0 \ll P$, Equation 2 reduces to the expression for the "characteristic age" of a pulsar,

$$\tau_c \equiv \frac{P}{2\dot{P}}. \tag{3}$$

Equation 3 often overestimates the true age of the system, indicating that P_0 is not much smaller than P (e.g., Migliazzo et al., 2002). PWNe resembling the Crab Nebula tend to be observed only for pulsars younger than about 20,000 years (see Section 4); older pulsars with high space velocities can power bow-shock PWNe (see Section 5).

In the case of a dipole magnetic field, we find $k = 2M_\perp^2/3Ic^3$, where $M_\perp$ is the component of the magnetic dipole moment orthogonal to the rotation axis. We can thus estimate an equatorial surface magnetic field strength:

$$B_p \equiv 3.2 \times 10^{19} (P\dot{P})^{1/2} \mathrm{G}, \tag{4}$$

where P is in seconds. Magnetic field strengths inferred from Equation 4 range between 10^8 G for recycled (or "millisecond") pulsars up to $>10^{15}$ G for "magnetars." Most pulsars with prominent PWNe have inferred magnetic fields in the range 1×10^{12} to 5×10^{13} G.

Annu. Rev. Astro. Astrophys. 2006.44:17-47. Downloaded from arjournals.annualreviews.org
by University of Bologna on 10/31/08. For personal use only.

2.1.2. Time evolution of $\dot{E}$ and P. A pulsar begins its life with an initial spin-down luminosity, $\dot{E}_0$. If n is constant, its spin-down luminosity then evolves with time, t, as (e.g., Pacini & Salvati 1973):

$$\dot{E} = \dot{E}_0 \left(1 + \frac{t}{\tau_0}\right)^{-\frac{(n+1)}{(n-1)}}, \tag{5}$$

where

$$\tau_0 \equiv \frac{P_0}{(n-1)\dot{P}_0} = \frac{2\tau_c}{n-1} - t \tag{6}$$

is the initial spin-down timescale of the pulsar. The pulsar thus has roughly constant energy output until a time τ_0, beyond which $\dot{E} \propto t^{-(n+1)/(n-1)}$. The spin period evolves similarly:

$$P = P_0 \left(1 + \frac{t}{\tau_0}\right)^{\frac{1}{n-1}}, \tag{7}$$

so that $P \approx P_0$ for $t \ll \tau_0$, but at later times $P \propto t^{1/(n-1)}$.

2.2. Radio and X-Ray Emission from Pulsar Wind Nebulae

As discussed in Section 4.1, the resultant deposition of energy with time generates a population of energetic electrons and positrons, which in turn powers a synchrotron-emitting nebula. Radio synchrotron emission is characterized by a power-law distribution of flux, such that $S_\nu \propto \nu^\alpha$, where S_ν is the observed flux density at frequency ν, and α is the source's "spectral index." At X-ray energies, the emission is often described as a power-law distribution of photons, such that $N_E \propto E^{-\Gamma}$, where N_E is the number of photons emitted between energies E and $E + dE$, and $\Gamma \equiv 1 - \alpha$ is the "photon index." Typical indices for PWNe are $-0.3 \lesssim \alpha \lesssim 0$ in the radio band, and ($\Gamma \approx 2$) in the X-ray band. This steepening of the spectrum implies one or more spectral breaks between these two wavebands, as discussed in Section 4.6.

If the distance to a PWN is known, the radio and X-ray luminosities, L_R and L_X, respectively, can be calculated over appropriate wavelength ranges. Typical ranges are 100 MHz to 100 GHz for L_R and 0.5–10 keV for L_X. Observed values for L_R and L_X span many orders of magnitude, but representative values might be $L_R \sim 10^{34}$ ergs s^{-1} and $L_X \sim 10^{35}$ ergs s^{-1}. The efficiency of conversion of spin-down luminosity into synchrotron emission is defined by efficiency factors $\eta_R \equiv L_R/\dot{E}$ and $\eta_X \equiv L_X/\dot{E}$. Typical values are $\eta_R \approx 10^{-4}$ and $\eta_X \approx 10^{-3}$ (Frail & Scharringhausen 1997; Becker & Trümper 1997), although wide excursions from this are observed. Note that if the synchrotron lifetime of emitting particles is a significant fraction of the PWN age (as is almost always the case at radio wavelengths, and sometimes also in X rays), then the PWN emission represents an integrated history of the pulsar's spin down, and η_R and η_X are not true instantaneous efficiency factors.

3. PULSAR WIND NEBULA EVOLUTION

We now consider the phases of evolution that govern the overall observational properties of PWNe. The detailed theoretical underpinning for these evolutionary phases is given in studies by Reynolds & Chevalier (1984), Chevalier (1998 2005), Blondin, Chevalier & Frierson (2001), Bucciantini et al. (2003), and van der Swaluw, Downes & Keegan (2004).

ISM: interstellar medium

We defer a discussion of the details of how the wind is generated to Section 4, and here simply assume that the pulsar's continuous energy injection ultimately results in an outflowing wind that generates synchrotron emission.

3.1. Expansion into Unshocked Ejecta

Because a pulsar is formed in a SN explosion, the star and its PWN are initially surrounded by an expanding SNR. The SNR blast wave at first moves outward freely at a speed $> (5 - 10) \times 10^3$ km s^{-1}, while asymmetry in the SN explosion gives the pulsar a random space velocity of typical magnitude 400–500 km s^{-1}. At early times the pulsar is thus located near the SNR's center.

The pulsar is embedded in slowly moving unshocked ejecta from the explosion and, as $t \ll \tau_0$, has constant energy output so that $\dot{E} \approx \dot{E}_0$ (see Equation 5). The pulsar wind is highly over-pressured with respect to its environment, and the PWN thus expands rapidly, moving supersonically and driving a shock into the ejecta. In the spherically symmetric case, the PWN evolves as (Chevalier 1977):

$$R_{PWN} \approx 1.5 \dot{E}_0^{1/5} E_{SN}^{3/10} M_{ej}^{-1/2} t^{6/5}$$
$$= 1.1\mathrm{pc} \left(\frac{\dot{E}_0}{10^{38}\ \mathrm{ergs\,s^{-1}}} \right)^{1/5} \left(\frac{E_{SN}}{10^{51}\ \mathrm{ergs}} \right)^{3/10} \left(\frac{M_{ej}}{10\ \mathrm{M_\odot}} \right)^{-1/2} \left(\frac{t}{10^3\ \mathrm{years}} \right)^{6/5}, \quad (8)$$

where R_{PWN} is the radius of the PWN's forward shock at time t, and E_{SN} and M_{ej} are the kinetic energy and ejected mass, respectively, released in the SN.

Because the PWN expansion velocity is steadily increasing, and the sound speed[3] in the relativistic fluid in the nebular interior is $c/\sqrt{3}$, the PWN remains centered on the pulsar. Observationally, we expect to see a rapidly expanding SNR, with a reasonably symmetric PWN near its center, and a young pulsar near the center of the PWN. A good example of a system at this stage of evolution is the recently discovered pulsar J1833-1034, which powers a bright X-ray and radio PWN, which in turn lies at the center of the young SNR G21.5–0.9 (**Figure 2*a***; Matheson & Safi-Harb 2005; Gupta et al., 2005; Camilo et al., 2006). This system is estimated to be ∼1000 years old.

3.2. Interaction with the Supernova Remnant Reverse Shock

As the expanding SNR sweeps up significant mass from the ISM or circumstellar medium, it begins to evolve into the "Sedov-Taylor" phase, in which the total energy

[3]This assumes that the bulk of the PWN is particle dominated (see Section 4.1).

Annu. Rev. Astro. Astrophys. 2006.44:17-47. Downloaded from arjournals.annualreviews.org
by University of Bologna on 10/31/08. For personal use only.

is conserved and is partitioned equally between kinetic and thermal contributions (see Truelove & McKee 1999, for a detailed discussion).

The region of interaction between the SNR and its surroundings now takes on a more complex structure, consisting of a forward shock where ambient gas is compressed and heated, and a reverse shock where ejecta are decelerated. The two shocks are separated by a contact discontinuity at which instabilities can form. The reverse shock at first expands outward behind the forward shock, but eventually moves inward. In the absence of a central pulsar or PWN, and assuming that the SNR is expanding into a constant density medium (which, given the effects of progenitor mass loss by stellar winds, may not be the case; see Chevalier 2005), the reverse shock reaches the SNR center in a time (Reynolds & Chevalier 1984):

$$t_{Sedov} \approx 7 \left(\frac{M_{ej}}{10\ M_{\odot}} \right)^{5/6} \left(\frac{E_{SN}}{10^{51}\ \mathrm{ergs}} \right)^{-1/2} \left(\frac{n_0}{1\ \mathrm{cm}^{-3}} \right)^{-1/3} \mathrm{kyr}, \qquad (9)$$

where n_0 is the number density of ambient gas. At this point the SNR interior is entirely filled with shock-heated ejecta, and the SNR is in a fully self-similar state that can be completely described by a small set of simple equations (Cox 1972). The radius of the shell's forward shock now evolves as $R_{SNR} \propto t^{2/5}$.

In the presence of a young pulsar, the inward moving SNR reverse shock collides with the outward moving PWN forward shock after a time $t_{coll} < t_{Sedov}$, typically a few thousand years (van der Swaluw et al., 2001; Blondin, Chevalier & Frierson 2001). Even in the simplest case of a stationary pulsar, an isotropic wind, and a spherical SNR, the evolution is complex. The reverse shock compresses the PWN by a large factor, which responds with an increase in pressure and a sudden expansion. The system reverberates several times, resulting in oscillation of the nebula on a timescale of several thousand years and a sudden increase in the nebular magnetic field that serves to burn off the highest energy electrons (Reynolds & Chevalier 1984; van der Swaluw et al., 2001; Bucciantini et al., 2003). The crushing of the PWN produces Rayleigh-Taylor instabilities, which can produce a chaotic, filamentary structure and mixing of thermal and nonthermal material within the PWN (Chevalier 1998; Blondin, Chevalier & Frierson 2001).

In a more realistic situation, the pulsar's motion carries it away from the SNR's center by the time the reverse shock collides with the PWN. Furthermore, if the SNR has expanded asymmetrically, then the reverse shock moves inward faster on some sides than on others. This results in a complicated three-dimensional interaction, spread over a significant time interval, during and after which the PWN can take on a highly distorted morphology and be significantly displaced from the pulsar position (Chevalier 1998; van der Swaluw, Downes & Keegan 2004). An example of such a system is the Vela SNR, shown in **Figure 3*a***.

3.3. A Pulsar Wind Nebula Inside a Sedov Supernova Remnant

Once the reverberations between the PWN and the SNR reverse shock have faded, the pulsar can again power a steadily expanding bubble. However, the PWN now

Annu. Rev. Astro. Astrophys. 2006.44:17-47. Downloaded from arjournals.annualreviews.org
by University of Bologna on 10/31/08. For personal use only.

Annu. Rev. Astro. Astrophys. 2006.44:17-47. Downloaded from arjournals.annualreviews.org
by University of Bologna on 10/31/08. For personal use only.

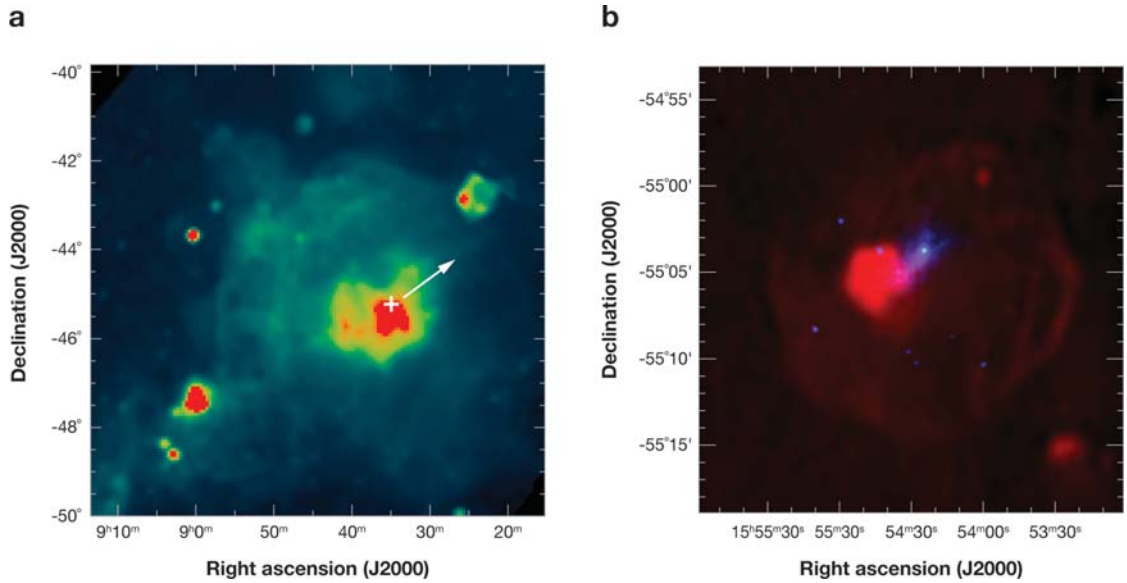

Figure 3

(*a*) A 2.4-GHz Parkes map of the Vela supernova remnant (SNR) (G263.9–3.3) (Duncan et al., 1996). A limb-brightened shell and a central radio pulsar wind nebula (PWN) can both be seen. The cross indicates the location of the associated pulsar B0833-45, whereas the white arrow indicates its direction of motion (Dodson et al., 2003). The fact that the pulsar is neither at nor moving away from the PWN's center indicates that a reverse shock interaction has taken place. (*b*) The composite SNR G327.1–1.1. An 843 MHz Molonglo image is shown in red (Whiteoak & Green 1996), and a 0.2–12 keV *XMM-Newton* image is in blue. The radio morphology consists of a faint shell enclosing a central PWN. The peak of X-ray emission indicates the likely position of an (as yet undetected) pulsar. The offset between the X-ray and radio nebulae indicates that the radio nebula is a "relic PWN" as discussed in Section 3.3. The pulsar is likely to be still moving subsonically through the SNR interior, generating a new PWN as it moves away from its birthsite.

expands into hot, shocked, ejecta at subsonic speeds, and no longer accelerates. In the spherically symmetric case, there are two solutions, depending on whether $t < \tau_0$ or $t > \tau_0$ (see Equation 6). In the former case, $\dot{E}$ is approximately constant and the PWN radius evolves as $R_{PWN} \propto t^{11/15}$ (van der Swaluw et al., 2001), whereas for the latter situation $\dot{E}$ is decaying, and (for $n = 3$) we expect $R_{PWN} \propto t^{3/10}$ (Reynolds & Chevalier 1984).

At this point, the distance traveled by the pulsar from the explosion site can become comparable to or even larger than the radius of an equivalent spherical PWN around a stationary pulsar. The pulsar thus escapes from its original wind bubble, leaving behind a "relic PWN," and generating a new, smaller PWN around its current position (van der Swaluw, Downes & Keegan 2004). Observationally, this appears as a central, possibly distorted radio PWN, showing little corresponding X-ray emission. The pulsar is to one side of or outside this region, with a bridge of radio and X-ray

emission linking it to the main body of the nebula. An example is the PWN in the SNR G327.1–1.1, shown in **Figure 3*b***.

The sound speed in the shocked ejecta drops as the pulsar moves from the center to the edge of the SNR. Eventually the pulsar's space motion becomes supersonic, and it now drives a bow shock through the SNR interior (Chevalier 1998; van der Swaluw, Achterberg & Gallant 1998). The ram pressure resulting from the pulsar's motion tightly confines the PWN, so that the nebula's extent is small, $\lesssim$1 pc. Furthermore, the pulsar wind is in pressure equilibrium with its surroundings, so that the PWN no longer expands steadily with time.

For a SNR in the Sedov phase, the transition to a bow shock takes place when the pulsar has moved 68% of the distance between the center and the forward shock of the SNR (van der Swaluw, Achterberg & Gallant 1998; van der Swaluw et al., 2003). The pulsar is now surrounded by a Mach cone, and the PWN takes on a cometary appearance at X-ray and radio wavelengths. An example of such a system is PSR B1853+01 in the SNR W44, as shown in **Figure 4*a***.

Annu. Rev. Astro. Astrophys. 2006.44:17-47. Downloaded from arjournals.annualreviews.org
by University of Bologna on 10/31/08. For personal use only.

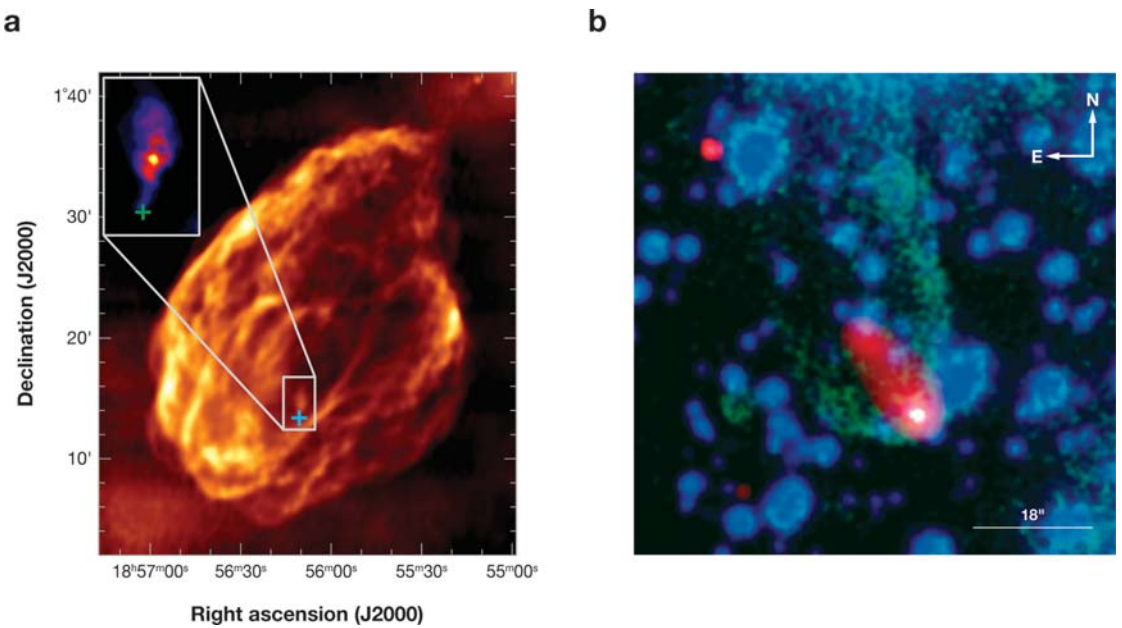

Figure 4

(*a*) The supernova remnant (SNR) W44 (G34.7–0.4). The main panel shows a 1.4 GHz VLA image of the SNR (Giacani et al., 1997), while the inset shows 8.4 GHz VLA data on the region surrounding the associated young pulsar B1853+01 (Frail et al., 1996), whose position is marked by a cross. The pulsar is nearing the edge of the SNR, and now drives a small bow-shock pulsar wind nebula as a result of its supersonic motion. (*b*) The recycled "Black Widow" pulsar (PSR B1957+20) and its bow shock (Stappers et al., 2003). The green shows Hα emission imaged with the Anglo-Australian Observatory, and the red shows X-ray emission observed with *Chandra* (the *blue* emission indicates background stars). The pulsar is moving at a position angle of 212° (north through east).

A pulsar will typically cross its SNR shell after ∼40,000 years (see Equation 15 in Section 5). If the SNR is still in the Sedov phase, the bow shock has a Mach number $\mathcal{M} \approx 3.1$ at this point (van der Swaluw et al., 2003). The injection of energy from the pulsar may brighten and re-energize the SNR shell during its passage (Shull, Fesen & Saken 1989; van der Swaluw, Achterberg & Gallant 2002).

3.4. A Pulsar in Interstellar Gas

Once outside its SNR, a pulsar's motion is often highly supersonic in interstellar gas. A bow-shock PWN results, with a potentially large Mach number, $\mathcal{M} \gg 1$.

In cases where the pulsar propagates through neutral gas, the forward shock driven by the PWN is visible, in the form of Hα emission produced by shock excitation and charge exchange (see Section 5.2). The shocked wind also produces synchrotron emission, resulting in a bright head and cometary tail, both best seen in radio and X rays (see Section 5.3). An example of an interstellar bow shock is the structure seen around PSR B1957+20, show in **Figure 4*b***.

As the pulsar now moves through the Galaxy, its $\dot{E}$ drops, and its motion carries it away from the denser gas in the Galactic plane where most neutron stars are born. Eventually most pulsars will end up with low spin-down luminosities in low density regions, where they may no longer be moving supersonically and their energy output is insufficient to power an observable synchrotron nebula. In this final stage, a pulsar is surrounded by a static or slowly expanding cavity of relativistic material with a radius $\gg$1 pc and confined by the thermal pressure of the ISM (Blandford et al., 1973; Arons 1983). Deep searches have yet to detect such "ghost nebulae" (e.g., Gaensler et al., 2000).

An alternate evolutionary path may take place for old pulsars in binary systems, which can eventually be spun up via accretion from a companion. This produces a recycled pulsar with a low value of $\dot{P}$ but a very rapid spin period, $P \sim 1 - 10$ ms. Such pulsars can have spin-down luminosities as high as $\dot{E} \approx 10^{34} - 10^{35}$ ergs s^{-1}, which is sufficient to generate observable bow-shock nebulae, as shown in **Figure 4*b***.

4. YOUNG PULSAR WIND NEBULAE

4.1. Pulsar Winds

Despite more than 35 years of work on the formation of pulsar winds, there are still large gaps in our understanding. The basic picture is that a charge-filled magnetosphere surrounds the pulsar, and that particle acceleration occurs in the collapse of charge-separated gaps either near the pulsar polar caps or in outer regions that extend to the light cylinder (i.e., to $R_{\rm LC} = c/\Omega$). The maximum potential generated by the rotating magnetic field has been calculated for the case of an aligned rotator (i.e., with the magnetic and spin axes co-aligned) by Goldreich & Julian (1969) as:

$$\Delta\Phi \approx \frac{B_p \Omega^2 R_{NS}^3}{2c} \approx 6 \times 10^{12} \left(\frac{B_p}{10^{12}\ \mathrm{G}}\right)\left(\frac{R_{NS}}{10\ \mathrm{km}}\right)^3 \left(\frac{P}{1\ \mathrm{s}}\right)^{-2} \mathrm{V}, \qquad (10)$$

Annu. Rev. Astro. Astrophys. 2006.44:17-47. Downloaded from arjournals.annualreviews.org
by University of Bologna on 10/31/08. For personal use only.

where R_{NS} is the neutron star radius. The associated particle current is $\dot{N}_{GJ} \approx (\Omega^2 B_p R_{NS}^3)/Zec$, where Ze is the ion charge. This current, although considerably modified in subsequent models, provides the basis for the pulsar wind. In virtually all models, the wind leaving the pulsar magnetosphere is dominated by the Poynting flux, $F_{E\times B}$, with a much smaller contribution from the particle energy flux, $F_{\rm particle}$. The magnetization parameter, σ, is defined as (e.g., Kennel & Coroniti 1984):

$$\sigma \equiv \frac{F_{E\times B}}{F_{\rm particle}} = \frac{B^2}{4\pi\rho\gamma c^2}, \tag{11}$$

where B, ρ, and γ are the magnetic field, mass density of particles, and Lorentz factor, in the wind, respectively. As the wind flows from the pulsar light cylinder, typical values of $\sigma > 10^4$ are obtained (see Arons 2002). However, models for the structure of the Crab Nebula (Rees & Gunn 1974; Kennel & Coroniti 1984a) require $\sigma \ll 1$ just behind the termination shock (see Section 4.3), in order to meet flow and pressure boundary conditions at the outer edge of the PWN. The high ratio of the synchrotron luminosity to the total spin-down power also requires a particle-dominated wind (Kennel & Coroniti 1984b), and implies $\gamma \sim 10^6$, a value considerably higher than that expected in the freely expanding wind (Arons 2002). Between the pulsar light cylinder and the position of the wind termination shock, the nature of the wind must thus change dramatically, although the mechanism for this transition is as yet unclear (see Melatos 1998; Arons 2002).

The loss of electrons from the polar regions of the star represents a net current that needs to be replenished to maintain charge neutrality. This may occur through ion outflow in equatorial regions. As discussed in Section 4.4, ions may contribute to nonthermal electron acceleration in the inner regions of the PWN.

4.2. Observed Properties of Young Pulsar Wind Nebulae

The deceleration of a pulsar-driven wind as it expands into the confines of cold, slowly expanding supernova ejecta produces a wind termination shock, at which electron/positron pairs are accelerated to ultrarelativistic energies (see Section 4.3). As these particles move through the wound-up magnetic field that comprises the PWN, they produce synchrotron radiation from radio wavelengths to beyond the X-ray band. For a power-law electron spectrum, the constant injection of particles plus a finite synchrotron-emitting lifetime lead to a spectral break at a frequency (Ginzburg & Syrovatskii 1965):

$$\nu_b = 10^{21}\left(\frac{B_{\rm PWN}}{10^{-6}\ {\rm G}}\right)^{-3}\left(\frac{t}{10^3\ {\rm years}}\right)^{-2}\ {\rm Hz}, \tag{12}$$

where $B_{\rm PWN}$ is the nebular magnetic field strength. Particles radiating at frequencies beyond ν_b reach the outer portions of the PWN in ever-diminishing numbers; most radiate their energy before they are able to travel that far. The result is that the size of the PWN decreases with increasing frequency, as is clearly observed in the Crab Nebula (**Figure 1**). For PWNe with low magnetic fields, the synchrotron loss times

Annu. Rev. Astro. Astrophys. 2006.44:17-47. Downloaded from arjournals.annualreviews.org
by University of Bologna on 10/31/08. For personal use only.

Annu. Rev. Astro. Astrophys. 2006.44:17-47. Downloaded from arjournals.annualreviews.org
by University of Bologna on 10/31/08. For personal use only.

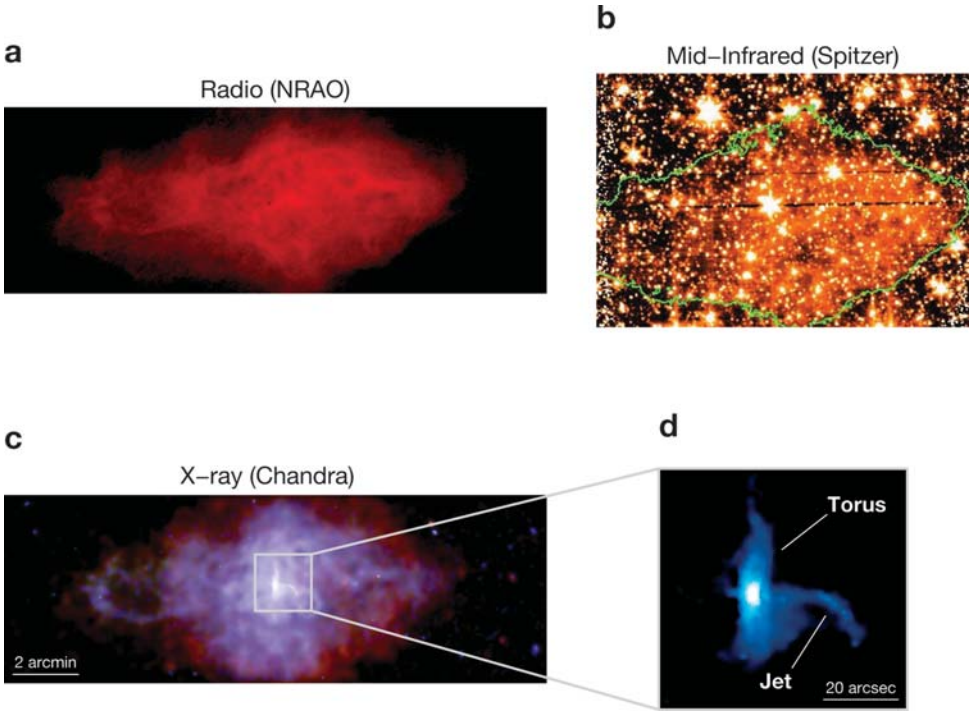

Figure 5

Images of the pulsar wind nebula 3C 58 (G130.7+3.1). (*a*) Radio synchrotron emission from the confined wind, with filamentary structure (Reynolds & Aller 1988). (*b*) Infrared synchrotron emission with morphology similar to the radio nebula (whose outer contour is shown in *green*). (*c*) X-ray synchrotron emission (*blue*), thermal emission (*red*) from shock-heated ejecta, and central torus/jet structure, shown expanded in panel *d* (Slane et al., 2004). Images are shown with north up and east to the left. The scale for the figures is indicated by the 2 arcmin scale bar except for panel *d*, where the 20 arcsec scale bar applies.

are longer and there may not be a significant difference in size between the radio and higher frequency bands (e.g., 3C 58 in **Figure 5**).

The morphology of a young PWN is often elongated along the pulsar spin axis due to the higher equatorial pressure associated with the toroidal magnetic field (Begelman & Li 1992; van der Swaluw 2003). This effect is seen clearly in many PWNe (e.g., **Figures 1** and **5**) and allows one to infer the likely projected orientation of the pulsar. As the nebula expands (see Section 3.1), Rayleigh-Taylor instabilities form as the fast-moving relativistic fluid encounters and accelerates slower-moving unshocked supernova ejecta. These form dense, finger-like filamentary structures that suffer photoionization from the surrounding synchrotron emission and radiate recombination lines in the optical and ultraviolet (UV) bands (**Figure 1*b***; Hester et al., 1996). The increased density compresses the magnetic field around the filaments, causing enhanced synchrotron emission. One thus observes radio structures that correspond to the optical/UV filaments.

Annu. Rev. Astro. Astrophys. 2006.44:17-47. Downloaded from arjournals.annualreviews.org
by University of Bologna on 10/31/08. For personal use only.

At the core of the PWN lies the pulsar itself. As its free-flowing equatorial wind encounters the more slowly-expanding nebula, a termination shock is formed. Particles accelerated at the shock form a toroidal structure, while some of the flow is collimated at speeds of $\sim 0.5c$ along the rotation axis, possibly contributing to the formation of jet-like structures (Bogovalov et al., 2005). These structures generate synchrotron radiation that is observed most readily in the X-ray band (**Figure 1*d***), although a toroid is also observed in optical images of the Crab Nebula (Hester et al., 1995). The emission pattern from jets or ring-like structures, as well as the larger scale geometry of the PWN, thus provides an indication of the pulsar's orientation. As we discuss in Section 4.4, the emission structures in the postshock and jet regions provide direct insight on particle acceleration, magnetic collimation, and the magnetization properties of the winds in PWNe. In addition, for pulsars whose proper motion is known, constraints on mechanisms for producing this population's high-velocity birth kicks can be derived based on the degree of alignment between the pulsar spin axis and the direction of motion (Lai, Chernoff & Cordes 2001; Ng & Romani 2004).

4.3. The Wind Termination Shock

The highly relativistic pulsar wind and its wound-up toroidal magnetic field inflate an expanding bubble whose outer edge is confined by the expanding shell of SN ejecta. As the wind is decelerated to match the boundary condition imposed by the more slowly-expanding ambient material at the nebula radius, a wind termination shock is formed at the radius, R_w, at which the ram pressure of the wind is balanced by the internal pressure of the PWN (**Figure 2*b***):

$$R_w = \sqrt{\dot{E}/(4\pi\omega c\,\mathcal{P}_{\rm PWN})}, \tag{13}$$

where ω is the equivalent filling factor for an isotropic wind, and $\mathcal{P}_{\rm PWN}$ is the total pressure in the shocked nebular interior. Upstream of the termination shock, the particles do not radiate, but flow relativistically along with the frozen-in magnetic field. At the shock, particles are thermalized and reaccelerated, producing synchrotron emission in the downstream flow. From estimates of the field strength, the observed X-ray emission implies Lorentz factors $\gamma \gtrsim 10^6$ in the shock.

A reasonable pressure estimate can be obtained by integrating the broad-band spectrum of the PWN, using standard synchrotron theory (Ginzburg & Syrovatskii 1965), and assuming equipartition between particles and the magnetic field. Typical $\mathcal{P}_{\rm PWN}$ and $\dot{E}$ values yield termination shock radii of order 0.1 pc, implying an angular size of several arcsec at distances of a few kiloparsecs. For the Crab Nebula, the equipartition field is $B_{\rm PWN} \approx 300$ μG (Trimble 1982), and the pressure reaches equipartition at a radius of $\sim(5-20)R_w$ (Kennel & Coroniti 1984a). The associated spin-down luminosity, $\dot{E} = 5 \times 10^{38}$ ergs s^{-1}, yields $R_w \sim 4 \times 10^{17}$ cm, consistent with the position of the optical wisps and the radius of the X-ray ring seen in **Figure 1*d***. Similar calculations indicate a much weaker field, $B_{\rm PWN} \approx 80$ μG in 3C 58 (Green & Scheuer 1992), yielding a termination shock radius similar to the

Crab, $R_w \sim 6 \times 10^{17}$ cm, given the smaller $\dot{E}$ of the pulsar. Indeed structure that possibly corresponds to the termination shock is seen at this separation from the pulsar (Slane, Helfand & Murray 2002). This lower field strength is also consistent with the fact that the observed size of 3C 58 is similar in the radio and X-ray bands (**Figure 5**).

It must be noted that high resolution X-ray observations of 3C 58 (Slane, Helfand & Murray 2002), G21.5–0.9 (Camilo et al., 2006), G292.0+1.8 (Hughes et al., 2001), and many other young PWNe and SNRs do not reveal directly the ring-like emission that is observed just outside the termination shock in the Crab pulsar, as seen in **Figure 1*d***. Rather, the compact emission around the pulsar appears slightly extended (see **Figure 5*d***), possibly originating from regions similar to the Crab Nebula's torus, downstream from the termination shock. However, the extent of such emission still provides a lower limit on $\mathcal{P}_{\rm PWN}$, as well as an indication of the pulsar orientation.

4.4. Formation of Tori, Jets, and Wisps

The geometry implied by the X-ray morphology of the Crab Nebula (see **Figure1*d***) is a tilted torus, with a jet of material that flows along the toroid axis, extending nearly 0.25 pc from the pulsar. A faint counter-jet accompanies the structure, and the X-ray emission is significantly enhanced along one edge of the torus. Both effects are presumably the result of Doppler beaming of the outflowing material, whereby the X-ray intensity, I, varies with viewing angle as (Pelling et al., 1987):

$$\frac{I}{I_0} = \left[\frac{\sqrt{1-\beta^2}}{1-\beta\cos\phi}\right]^{\Gamma+1}, \qquad (14)$$

where βc is the flow speed immediately downstream of the termination shock, ϕ is the angle of the flow to the line of sight, and I_0 is the unbeamed intensity.

Similar geometric structures are observed in G54.1+0.3, for which *Chandra* observations reveal a central point-like source surrounded by an X-ray ring whose geometry suggests an inclination angle of about 45° (Lu et al., 2002). The X-ray emission is brightest along the eastern limb of the ring. If interpreted as the result of Doppler boosting, this implies a postshock flow velocity of $\sim 0.4c$. The ring is accompanied by faint bipolar elongations aligned with the projected axis of the ring, consistent with the notion that these are jets of shocked material flowing along the pulsar rotation axis. The total luminosity of these structures is similar to that of the central ring. This is to be contrasted with the Crab and 3C 58 (**Figures 1** and **5**), for which the torus outshines the jets by a large factor. Moreover, for G54.1+0.3 the brighter portion of the outflow lies on the same side of the pulsar as the brightest portion of the ring, which is inconsistent with Doppler boosting. A similarly troubling observation is that the brightness distribution around the inner ring of the Crab also fails to show Doppler brightening consistent with that seen in its surrounding torus; the brightness is reasonably uniform except for some compact structures that vary in position and brightness with time (see Section 4.5).

Annu. Rev. Astro. Astrophys. 2006.44:17-47. Downloaded from arjournals.annualreviews.org
by University of Bologna on 10/31/08. For personal use only.

Annu. Rev. Astro. Astrophys. 2006.44:17-47. Downloaded from arjournals.annualreviews.org
by University of Bologna on 10/31/08. For personal use only.

The formation of these jet/torus structures can be understood as follows. Outside the pulsar magnetosphere, the particle flow is radial. The rotation of the pulsar forms an expanding, toroidal, alternating magnetic field for which the Poynting flux varies as $\sin^2 \psi$, where ψ is the angle from the rotation axis. Conservation of energy flux along flow lines leads to a latitude dependence of the Lorentz factor of the wind of the form $\gamma = \gamma_0 + \gamma_m \sin^2 \psi$ (Bogovalov & Khangoulyan 2002), where γ_0 is the wind Lorentz factor just outside the light cylinder ($\gamma_0 \sim 10^2$ in standard models for pulsar winds; e.g., Daugherty & Harding 1982), and γ_m is the maximum Lorentz factor of the preshock wind particles ($\gamma_m \sim 10^6$ near the termination shock; Kennel & Coroniti 1984a). From Equation 11, we see that this corresponds to a latitude variation in the magnetization parameter also, with σ much larger at the poles than at the equator. This anisotropy results in the toroidal structure of the downstream wind. Moreover, modeling of the flow conditions across the shock shows that magnetic collimation produces jet-like flows along the rotation axis (Komissarov & Lyubarsky 2004; Bogovalov et al., 2005). This collimation is highly dependent on the magnetization of the wind. For $\sigma \gtrsim 0.01$, magnetic hoop stresses are sufficient to divert the toroidal flow back toward the pulsar spin axis, collimating and accelerating the flow to speeds of $\sim 0.5c$ (Del Zanna, Amato & Bucciantini 2004); smaller values of σ lead to an increase in the radius at which the flow is diverted. The launching points of the jets observed in the Crab Nebula, which appear to form much closer to the pulsar than the observed equatorial ring, apparently reflect such variations in the value of σ. Near the poles σ is large, resulting in a small termination shock radius and strong collimation, while near the equator σ is much smaller and the termination shock extends to larger radii (Bogovalov & Khangoulyan 2002).

Because γ is smaller at high latitudes, models for the brightness of the jet-like flows produced by the collimation process fall short of what is observed. However, kink instabilities in the toroidal field may transform magnetic energy into particle energy, thus accelerating particles and brightening the jet (Bogovalov et al., 2005). Such instabilities limit the duration of the collimation (Begelman 1998). Evidence for the effects of kink instabilities is seen in the curved nature of many PWN jets, particularly for the Vela PWN where the jet morphology is observed to change dramatically on timescales of months (Pavlov et al., 2003). There appears to be a wide variation in the fraction of $\dot{E}$ channeled into PWN jets, ranging from $\sim 2.5 \times 10^{-5}$ in 3C 58 to nearly 10^{-3} for the PWN powered by PSR B1509-58, based on their synchrotron spectra (Gaensler et al., 2002; Slane et al., 2004). This apparently indicates considerable differences in the efficiency with which additional acceleration occurs along the jets.

The torus surrounding the Crab pulsar is characterized by the presence of wisp-like structures (see **Figure 1*d***), whose position and brightness vary with time in the optical, infrared, and X-ray bands, and which emanate from the termination shock and move outward through the torus with inferred outflow speeds of $\sim 0.5c$ (Hester et al., 2002; Melatos et al., 2005). The exact nature of these structures is not fully understood. Hester et al. (2002) suggest that they are formed by synchrotron instabilities. However, the position of the arc-like structure surrounding PSR B1509-58 seems inconsistent with this hypothesis given the much lower magnetic field in the PWN (Gaensler et al., 2002). An alternative suggestion is that the wisps are the

sites of compression of the electron/positron pair plasma on scales of the cyclotron gyration radius of ions in the outflow (∼0.15 pc in the Crab Nebula), which can also explain the radius of the X-ray arc seen around PSR B1509-58 (Gallant & Arons 1994; Spitkovsky & Arons 2004, and references therein).

It is worth noting that VLA observations of the Crab Nebula show variable radio structures very similar to the optical and X-ray wisps, indicating that acceleration of the associated particles must be occurring in the same region as for the X-ray–emitting population (Bietenholz et al., 2004).

4.5. Filamentary and Compact Structures in Pulsar Wind Nebulae

In the Crab Nebula, an extensive network of filaments is observed in Hα, [OIII] and other optical lines, surrounding the nonthermal optical emission from the PWN (**Figure 1*b***). The detailed morphology and ionization structure of these filaments indicate that they form from Rayleigh-Taylor instabilities as the expanding relativistic bubble sweeps up and accelerates slower moving ejecta (Hester et al., 1996). Magnetohydrodynamic simulations support this picture, indicating that 60–75% of the swept-up mass can be concentrated in such filaments (Jun 1998; Bucciantini et al., 2004). As the expanding PWN encounters these filaments, compression increases the density and magnetic field strength, forming sheaths of enhanced synchrotron emission observed as a corresponding shell of radio filaments (Reynolds 1988). X-ray observations reveal no such filaments in the Crab Nebula (Weisskopf et al., 2000). This is presumably because the higher energy electrons required to produce the X-ray emission suffer synchrotron losses before reaching the outer regions of the PWN, consistent with the smaller extent of the nebula in X rays than in the radio.

A different picture is presented by X-ray observations of 3C 58, which reveal a complex of loop-like filaments most prominent near the central regions of the PWN, but evident throughout the nebula (**Figure 5*c***; Slane et al., 2004). These nonthermal X-ray structures align with filaments observed in the radio band (Reynolds & Aller 1988). Optical observations of 3C 58 also reveal faint filaments (van den Bergh 1978), whose origin is presumably similar to those in the Crab Nebula. However, a detailed X-ray/optical comparison shows that most of the X-ray filaments do not have optical counterparts. Although comparisons with deeper optical images are clearly needed, the fact that many of the X-ray features without optical counterparts are brighter than average suggests that these may actually arise from a different mechanism. Slane et al. (2004) propose that the bulk of the discrete structures seen in the X-ray and radio images of 3C 58 are magnetic loops torn from the toroidal field by kink instabilities. In the inner nebula, the loop sizes are similar to the size of the termination shock radius (∼0.1 pc), as suggested by Begelman (1998). As the structures expand, they enlarge slightly as a consequence of decreasing pressure.

There is also considerable loop-like filamentary structure evident in high resolution X-ray images of the Crab Nebula (**Figure 1*d***; Weisskopf et al., 2000). These filaments appear to wrap around the torus, perpendicular to the toroidal plane, and may be signatures of kink instabilities in the termination shock region.

Annu. Rev. Astro. Astrophys. 2006.44:17-47. Downloaded from arjournals.annualreviews.org
by University of Bologna on 10/31/08. For personal use only.

In some PWNe, compact knot-like structures are observed close to the pulsar, which dissipate and reappear on timescales of order months (Hester et al., 2002; Melatos et al., 2005). Examples can be seen for the Crab in **Figure 1*d***, and similar structures are also seen for PSR B1509-58 (Gaensler et al., 2002). Some of these features appear in projection inside the termination shock region. However, it is believed that they actually correspond to unstable, quasi-stationary shocks in the region just outside the termination shock, at high latitudes where the shock radius is small due to larger values of σ (e.g., Komissarov & Lyubarsky 2004).

4.6. Pulsar Wind Nebula Spectra

As noted in Section 2.2, the spectra of PWNe are characterized by a flat power law index at radio wavelengths ($\alpha \approx -0.3$) and a considerably steeper index in X rays ($\Gamma \approx 2$). (Recall that $\Gamma \equiv 1 - \alpha$.) The nature of this spectral steepening is not understood. Simple assumptions of a power-law particle spectrum injected by the pulsar would predict a power-law synchrotron spectrum, with a break associated with the aging of the particles (see Equation 12); the expected increase in spectral index is $\Delta\alpha = 0.5$, which is smaller than what is typically observed (Woltjer et al., 1997). Moreover, for many PWNe a change in spectral index is inferred at low frequencies that would imply unrealistically high magnetic fields (e.g., Green & Scheuer 1992). Relic breaks in the spectrum can be produced by a rapid decline in the pulsar output over time, and these breaks propagate to lower frequencies as the PWN ages (Pacini & Salvati 1973). The inherent spectrum of the injected particles, which may deviate from a simple power law, as well as modifications from discrete acceleration sites all contribute to a complicated integrated spectrum. As a result, the interpretation of spectral steepening as being due to synchrotron losses can lead to drastically wrong conclusions about PWN properties.

At frequencies for which the synchrotron lifetime is shorter than the flow time to the edge of the PWN, a steepening of the spectrum with radius is expected. Radial steepening is indeed observed in the X-ray spectra of the Crab Nebula, 3C 58, and G21.5–0.9 (Slane et al., 2000; Willingale et al., 2001; Slane et al., 2004), but the spectra steepen rather uniformly with radius, whereas generalizations of the Kennel & Coroniti (1984b) model predict a much more rapid steepening near the outer regions (Reynolds 2003). Some mixing of electrons of different ages at each radius seems to be required, perhaps due to diffusion processes in the PWN.

5. BOW SHOCKS AROUND HIGH VELOCITY PULSARS

Many pulsars are born with high space velocities, typically $V_{\rm PSR} = 400$–500 km s^{-1}, but for some sources exceeding 1000 km s^{-1}. These high velocities are almost certainly the result of kicks given to the star during or shortly after core collapse (Lai 2004). Young pulsars thus have the highest velocities of any stellar population, and many have sufficient speeds to eventually escape the Galaxy.

As discussed in Section 3.3, a pulsar's ballistic motion allows it to eventually escape its original PWN, and to propagate through the shocked ejecta in the SNR interior.

Annu. Rev. Astro. Astrophys. 2006.44:17-47. Downloaded from arjournals.annualreviews.org
by University of Bologna on 10/31/08. For personal use only.

At first the pulsar's motion will be subsonic in this hot gas, but by the time the pulsar nears the edges of the SNR, the sound speed drops sufficiently for the pulsar's motion to be supersonic. In the simplest situation of a spherical SNR in the Sedov phase, expanding into a uniform medium, this transition occurs at half the crossing time (given in Equation 15 below), at which point the pulsar has traveled 68% of the distance from the center of the SNR to its edge (van der Swaluw, Downes & Keegan 2004). This simple result is independent of $V_{\rm PSR}$, n_0, or E_{SN}. The pulsar's supersonic motion now produces a PWN with a bow shock morphology.

MHD: magnetohydrodynamic

Because the SNR is decelerating, the pulsar ultimately penetrates and then escapes the shell. A pulsar moving at $V_{\rm PSR} \gtrsim 650$ km s^{-1} will escape while the SNR is still in the Sedov phase, after a time (van der Swaluw et al., 2003):

$$t_{cross} = 44\left(\frac{E_{SN}}{10^{51}\text{ergs}}\right)^{1/3}\left(\frac{n_0}{1\text{ cm}^{-3}}\right)^{-1/3}\left(\frac{V_{\rm PSR}}{500\text{ km s}^{-1}}\right)^{-5/3}\text{kyr}. \quad (15)$$

At times $t > t_{cross}$, a pulsar proceeds to move through the ambient ISM.

The speed of sound in interstellar gas is a function of temperature: typical values are approximately 1, 10, and 100 km s^{-1} for the cold, warm, and hot components of the ISM, respectively. Thus, except in the case of a particularly slow moving pulsar moving through coronal gas, a pulsar will move supersonically and drive a bow shock through the ISM.

5.1. Theoretical Expectations

The pulsar wind in a bow shock is decelerated at a termination shock, just as for younger PWNe (see Section 4.3). However, the external source of pressure balance is now ram pressure from the pulsar's motion, rather than the internal pressure of the shocked wind. Furthermore, because ram pressure is not isotropic, the termination shock radius varies as a function of angle with respect to the pulsar's velocity vector. In the direction of the star's motion, the termination shock radius is referred to as the "stand-off distance," R_{w0}, and is defined by (cf. Equation 13):

$$\frac{\dot{E}}{4\pi\omega R_{w0}^2 c} = \rho_0 V_{\rm PSR}^2, \quad (16)$$

where ρ_0 is the ambient density. If the wind is isotropic and $\omega = 1$, then at a polar angle θ with respect to the bow shock's symmetry axis, the analytic solution for the termination shock radius as a function of position is (Wilkin 1996):

$$R_w(\theta) = R_{w0}\csc\theta\sqrt{3(1-\theta\cot\theta)}. \quad (17)$$

It is important to note that the above solution assumes an efficiently cooled thin-layer shock, in contrast to the double shock expected for pulsar bow shocks. Full hydrodynamic and MHD simulations show that Equation 17 is a reasonable approximation in regions near the apex ($\theta \lesssim \frac{\pi}{2}$), but performs more poorly further downstream (Bucciantini 2002a; van der Swaluw et al., 2003).

A result of such simulations is shown in **Figure 6*a***. The double-shock structure is clearly apparent, consisting of a forward shock where the ISM is heated, plus the

Annu. Rev. Astro. Astrophys. 2006.44:17-47. Downloaded from arjournals.annualreviews.org
by University of Bologna on 10/31/08. For personal use only.

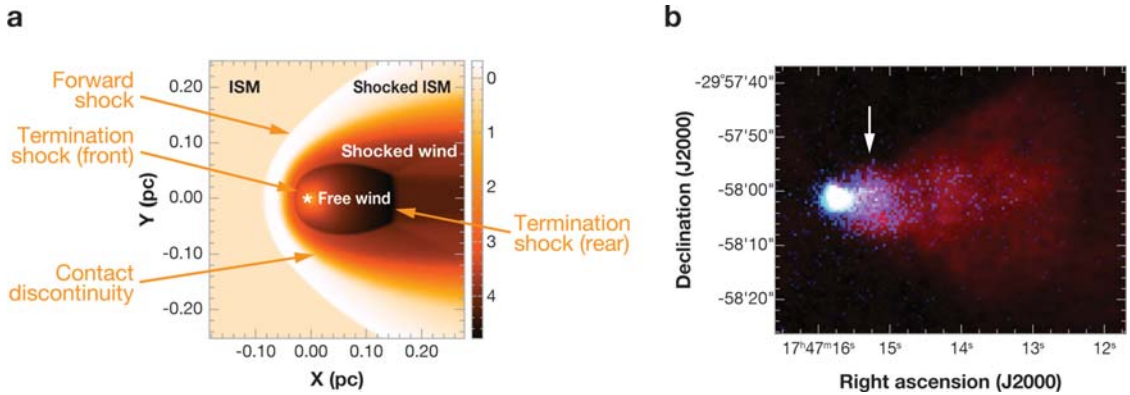

Figure 6

(*a*) A hydrodynamic simulation of a pulsar bow shock, adapted from Gaensler et al. (2004). The pulsar, whose position is marked with an asterisk, is moving from right to left with a Mach number $\mathcal{M} = 60$. The intensity in the image and the scale bar indicate density, in units of $\log_{10}(\rho_0/10^{-24}$ g cm$^{-3})$. (*b*) *Chandra* X-ray (*blue*) and VLA radio (*red*) images of G359.23–0.82 ("the Mouse"), the bow shock associated with PSR J1747-2958 (Gaensler et al., 2004). The white arrow marks a bright compact region of X-ray emission behind the apex, which possibly corresponds to the surface of the termination shock.

termination shock where the pulsar's wind decelerates. As expected, the termination shock is not of uniform radius around the pulsar: specifically, for low Mach numbers, $\mathcal{M} \sim 1 - 3$ [as may be appropriate for pulsars traveling supersonically inside their SNRs; see Section 3.3 and van der Swaluw, Downes & Keegan (2004)], the ratio of termination shock radii between polar angles $\theta = \pi$ and $\theta = 0$ is approximately $\mathcal{M}$ (Bucciantini 2002a; van der Swaluw et al., 2003), but for $\mathcal{M} \gg 1$ (typical of bow shocks in the ambient ISM; see Section 3.4), this ratio approaches a limit of $\sim 5 - 6$ (Gaensler et al., 2004; Bucciantini, Amato & Del Zanna 2005).

5.2. Observations: Forward Shock

If a pulsar drives a bow shock through neutral gas, then collisional excitation and charge exchange occur at the forward shock, generating optical emission in the Balmer lines (Bucciantini & Bandiera 2001; Bucciantini 2002b). Indeed several pulsar bow shocks have been identified in the 656-nm Hα line, associated with (in order of discovery) B1957+20 (**Figure 4*b***; Kulkarni & Hester 1988), B2224+65 ("the Guitar"; Cordes, Romani & Lundgren 1993), J0437-4715 (Bell et al., 1995), RX J1856.5-3754 (van Kerkwijk & Kulkarni 2001), B0740-28 (Jones, Stappers & Gaensler 2002), and J2124-3358 (Gaensler, Jones & Stappers 2002).

If the distance to the system is known, R_{w0} can be directly measured, provided that one adopts a scaling factor of $\sim 0.4 - 0.6$ to translate between the observed radius of the forward shock to that of the termination shock (Bucciantini 2002a; van der Swaluw et al., 2003). If $\dot{E}$ and $V_{\rm PSR}$ have been measured, Equation 16 can then be applied to yield ρ_0. This is an approximation, because $\omega = 1$ is usually assumed,

Annu. Rev. Astro. Astrophys. 2006.44:17-47. Downloaded from arjournals.annualreviews.org
by University of Bologna on 10/31/08. For personal use only.

and because of the unknown inclination of the pulsar's motion to the line of sight,[4] but certainly suggests ambient number densities $\sim$0.1 cm^{-3}, as expected for warm neutral ambient gas (Chatterjee & Cordes 2002; Gaensler, Jones & Stappers 2002). For pulsars for which $V_{\rm PSR}$ is not known, one can write:

$$\rho_0 V_{\rm PSR}^2 = \gamma_1 \mathcal{M}^2 \mathcal{P}_{\rm ISM}, \tag{18}$$

where $\gamma_1 = 5/3$ and $\mathcal{P}_{\rm ISM}$ are the adiabatic coefficient and pressure of the ISM, respectively. Estimates for $\mathcal{P}_{\rm ISM}$ and ω in Equations 16 and 18 then yield $\mathcal{M}$.

For the bow shocks associated with RX J1856.5-3754, PSR J0437-4715, and PSR B1957+20 (**Figure 4*b***), the shape of the forward shock is a good match to the solution predicted by Equation 17 and simulated in **Figure 6*a***. However, the optical emission around PSRs B2224+65, J2124-3358, and B0740-28 all show strong deviations from the expected shape in that there are abrupt kinks and inflection points in the Hα profile (Jones, Stappers & Gaensler 2002; Chatterjee & Cordes 2002). Furthermore, in the case of PSR J2124-3358 there is an apparent rotational offset between the symmetry axis of the bow shock and the velocity vector of the pulsar (Gaensler, Jones & Stappers 2002). These systems imply the presence of some combination of anisotropies in the pulsar wind (as are observed in young pulsars; see Section 4.4), gradients and fluctuations in the density of the ISM, or a bulk velocity of ambient gas with respect to the pulsar's local standard of rest. Extensions of Equation 17 to account for these effects have been presented by Bandiera (1993) and by Wilkin (2000), and have been applied to interpret the morphology of PSR J2124-3358 by Gaensler, Jones & Stappers (2002).

5.3. Observations: Termination Shock

Just as for the PWNe around the youngest pulsars discussed in Section 4.3, particles in the pulsar wind inside a bow shock will be accelerated at the termination shock, producing nonthermal synchrotron emission that can be potentially observed in the radio and X-ray bands. Indeed cometary radio and X-ray PWNe aligned with the direction of motion have been now identified around many pulsars, convincing examples of which include PSRs B1853+01 (**Figure 4*a***; Frail et al., 1996; Petre, Kuntz & Shelton 2002), B1957+20 (**Figure 4*b***; Stappers et al., 2003), and B1757-24 ("the Duck"; Frail & Kulkarni 1991; Kaspi et al., 2001).

The most spectacular example of this class is G359.23–0.82, the X-ray/radio bow shock powered by PSR J1747-2958 ("the Mouse"; Yusef-Zadeh & Bally 1987; Gaensler et al., 2004), multi-wavelength observations of which are shown in **Figure 6*b***. The extent of the radio trail in this system is larger than in X rays, reflecting the difference in synchrotron lifetimes between these bands (cf. Section 4.2).

The X-ray morphology of the Mouse in **Figure 6*b*** appears to consist of two components: a bright compact region extending $\sim$0.2 pc from the pulsar, superimposed

[4]Note that the correction factor for motion inclined to the line of sight cannot be derived through simple trigonometry (Gaensler, Jones & Stappers 2002).

Annu. Rev. Astro. Astrophys. 2006.44:17-47. Downloaded from arjournals.annualreviews.org
by University of Bologna on 10/31/08. For personal use only.

IC: inverse Compton

on a larger fainter component extending ∼1 pc from the pulsar. Comparison with the hydrodynamic simulation in **Figure 6*a*** suggests that the bright component of the X-ray emission corresponds to the surface of the wind termination shock, while fainter, more extended X-ray emission originates from the shocked wind (Gaensler et al., 2004). In this identification, the bright X-ray component of this bow shock corresponds to the inner toroidal rings discussed in Section 4.4, but are elongated due to the pulsar motion. This interpretation is supported by the fact that the extent of the termination shock region along the symmetry axis (in units of R_{w0}) should be a function of Mach number, as was discussed in Section 5.1. Indeed for the Mouse, with $\mathcal{M} \sim 60$ (Gaensler et al., 2004), this bright region is about twice as long (relative to R_{w0}) as for the pulsar bow shock seen inside the SNR IC 443 (Olbert et al., 2001), which must have $\mathcal{M} \lesssim 3$ because it is moving through shocked gas in the SNR interior (van der Swaluw et al., 2003).

In PWNe for PSRs B1757-24 (Kaspi et al., 2001) and B1957+20 (**Figure 4*b***; Stappers et al., 2003), only a short (∼0.1 pc) narrow X-ray trail is apparent. Such features have been interpreted as a rapid back-flow or nozzle, which transports particles downstream (Wang, Li & Begelman 1993; Kaspi et al., 2001). However, **Figure 6** suggests that the short trail seen behind PSRs B1757-24 and B1957+20 is the surface of the termination shock, and that emission from the post-shock wind further downstream is too faint to see (Gvaramadze 2004; Gaensler et al., 2004). Deeper X-ray observations are required to test this possibility.

Hydrodynamic models predict that the pulsar's motion should divide the post-shock emitting region of a bow shock into two distinct zones: a highly magnetized broad tail originating from material shocked at $\theta \lesssim \frac{\pi}{2}$, plus a more weakly magnetized, narrow, collimated tail, produced by material flowing along the axis $\theta \approx \pi$ (Bucciantini 2002a; Romanova, Chulsky & Lovelace 2005). These two structures are both apparent in the Mouse (Gaensler et al., 2004). Through relativistic MHD simulation, this and other issues related to the structure of the post-shock flow are now being explored (e.g., Bucciantini, Amato & Del Zanna 2005).

6. OTHER TOPICS AND RECENT RESULTS

6.1. Pulsars and Pulsar Wind Nebulae in Very Young Supernova Remnants

The youngest known Galactic PWNe are the Crab Nebula and 3C 58, powered by pulsars thought to correspond to the SNe of 1054 CE and 1181 CE, respectively.[5] It would be of great interest to identify PWNe at earlier evolutionary stages.

SN 1987A formed a neutron star, but deep searches have failed to detect a central object, down to a luminosity $\lesssim 10^{34}$ ergs s^{-1} (e.g., Graves et al., 2005). This is well below the luminosity of the Crab Nebula, and may indicate that the central neutron

[5]The association of 3C 58 with 1181 CE is not completely secure; see Stephenson & Green (2002) and Chevalier (2005), and references therein.

Annu. Rev. Astro. Astrophys. 2006.44:17-47. Downloaded from arjournals.annualreviews.org
by University of Bologna on 10/31/08. For personal use only.

star has collapsed further into a black hole, accretes from fall-back material, or does not generate a wind (e.g., Fryer, Colgate & Pinto 1999).

Searches for PWNe in other extragalactic SNe and SNRs have generally not produced any convincing candidates (Reynolds & Fix 1987; Bartel & Bietenholz 2005). However, recent high resolution radio images have revealed the gradual turn-on of a central flat-spectrum radio nebula in SN 1986J, which may correspond to emission from a very young PWN (Bietenholz, Bartel & Rupen 2004). New wide-field radio and X-ray images of other galaxies may lead to further identification of young PWNe, whereas optical and UV spectroscopy of recent SNe may identify PWNe through emission lines that broaden with time as gas is swept up by the expanding pulsar wind (Chevalier & Fransson 1992).

6.2. Winds from Highly Magnetized Neutron Stars

A growing population of neutron stars have surface magnetic fields (inferred via Equation 4) above the quantum critical limit of $B_p = 4.4 \times 10^{13}$ G. The properties of these stars indicate that they are comprised of two apparently distinct populations: the high-field radio pulsars (McLaughlin et al., 2003, and references therein), and the exotic magnetars (Woods & Thompson 2006). The winds and PWNe of these sources potentially provide a view of different spin-down processes than those seen in normal pulsars.

Most of the high-field radio pulsars have $\dot{E} \approx 10^{32} - 10^{34}$ ergs s^{-1}. For typical efficiency factors $\eta_R, \eta_X \lesssim 10^{-3}$, this implies PWNe too faint to be detectable. However, the very young pulsars J1846-0258 ($B_p = 4.9 \times 10^{13}$ G) and J1119-6127 ($B_p = 4.1 \times 10^{14}$ G) have high spin-down luminosities ($\dot{E} > 10^{36}$ ergs s^{-1}) and are near the centers of SNRs. In both cases PWNe are detected, although with very different properties. PSR J1846-0258 puts a large fraction ($\eta_X \sim 0.2$) of its spin-down power into a luminous X-ray PWN $\sim$2 pc in extent (Helfand, Collins & Gotthelf 2003), whereas PSR J1119-6127 powers an under-luminous ($\eta_X \sim 2 \times 10^{-4}$) and small ($\sim$0.2 pc) X-ray nebula (Gonzalez & Safi-Harb 2003). Clearly PWN properties are dominated by factors such as age, environment, and evolutionary state (see Section 3) rather than the associated pulsar's surface magnetic field.

Magnetars also spin down, albeit in some cases not smoothly (Woods et al., 2002). Just as for radio pulsars, this rotational energy output is thought to go into a relativistic wind, but traditional PWNe have not been detected around magnetars,[6] presumably because they have time-averaged spin down luminosities $\dot{E} \lesssim 10^{34}$ ergs s^{-1} for all these sources. Magnetars likely experience an enhanced torque over the dipole spin-down presumed to act in radio pulsars, as a result of either Alfvén waves and outflowing relativistic particles driven by seismic activity, or by a large-scale twist of the external magnetic field (Harding, Contopoulos & Kazanas 1999; Thompson, Lyutikov & Kulkarni 2002). Under either circumstance, the spin-down behavior deviates from that described in Equations 2 to 7 (e.g., Thompson et al., 2000).

[6]The magnetar SGR 1806–20 was originally presumed to power the radio nebula G10.0–0.3, but a revision in the position of this neutron star now makes this unlikely (Hurley et al., 1999).

Annu. Rev. Astro. Astrophys. 2006.44:17-47. Downloaded from arjournals.annualreviews.org
by University of Bologna on 10/31/08. For personal use only.

A transient radio PWN was proposed to account for the short-lived radio nebula seen in 1998 following the giant flare from the magnetar SGR 1900+14 (Frail, Kulkarni & Bloom 1999). However, recent observations of a radio nebula in the aftermath of a giant flare from SGR 1806-20 suggest that the synchrotron emission from these nebulae is powered by ejected baryonic material, so that these sources are more analogous to SNRs than to PWNe (Gaensler et al., 2005).[7]

6.3. TeV Observations of Pulsar Wind Nebulae

The Crab Nebula is a well-known source of TeV gamma-rays (Weekes et al., 1989, and references therein). This emission is well explained as inverse Compton emission, the relativistic particles in the shocked wind acting as scattering centers for the synchrotron photons that they themselves emit at lower energies (Atoyan & Aharonian 1996). Under this interpretation, the emitted spectrum can be modeled to provide the mean and spatial distribution of the nebular magnetic field strength, and hence the PWN's particle content, the time-averaged injection rate of particles, and an independent estimate of the magnetization parameter, σ (e.g., de Jager et al., 1996). The estimated values of $B_{\rm PWN}$ and σ are in good agreement with those derived from the MHD model of Kennel & Coroniti (1984a).

The new generation of ground-based Čerenkov detectors (most notably the High Energy Stereoscopic System, HESS) has now begun to detect other PWNe in the TeV band. These detections indicate that acceleration of particles to considerable energies must have occurred and provide estimates of the nebular magnetic field strength, which can be used in modeling and interpreting the other nebular structures discussed in Section 4. The much lower synchrotron luminosities of these other sources compared to the Crab Nebula imply that the seed photons for IC scattering are in these cases primarily external, originating from a combination of the cosmic microwave background and a local contribution from dust and starlight. Recent TeV detections of PWNe by HESS include G0.9+0.1 and G320.4–1.2/PSR B1509-58 (Aharonian et al., 2005a, b). As shown in **Figure 7**, the latter is spatially resolved by HESS and has a TeV morphology that is a good match to the X-ray synchrotron nebula. Such observations can potentially provide direct measurements of spatial variations in the magnetic fields of PWNe.

6.4. Pulsar Winds in Binary Systems

The recently discovered dual-line double pulsar PSR J0737-3039 consists of a 23-ms pulsar ("A") and a 2.8-s pulsar ("B") in a 2.4-hour orbit, viewed virtually edge-on (Lyne et al., 2004). This system is proving to be a remarkable new probe of pulsars and their winds, providing information at much closer separations to the pulsar than is possible for the sources discussed in Sections 4 and 5.

[7]A possibly transient radio source has also recently been identified coincident with the flaring magnetar XTE J1810-197, but the nature of this source is as yet unclear (Halpern et al., 2005).

Annu. Rev. Astro. Astrophys. 2006.44:17-47. Downloaded from arjournals.annualreviews.org
by University of Bologna on 10/31/08. For personal use only.

Annu. Rev. Astro. Astrophys. 2006.44:17-47. Downloaded from arjournals.annualreviews.org
by University of Bologna on 10/31/08. For personal use only.

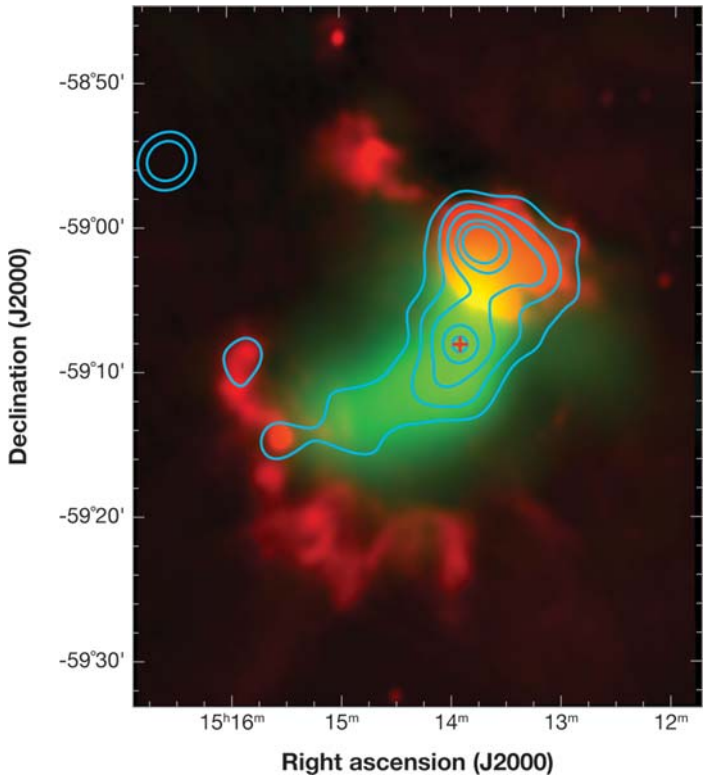

Figure 7

Multiwavelength images of the pulsar wind nebula (PWN) powered by the young pulsar B1509-58. *ROSAT* PSPC data (in *blue contours* at levels of 5%, 10%, 20%, 40%, and 60% of the peak) show the extent of the X-ray PWN (Trussoni et al., 1996), while 843 MHz Molonglo data (in *red*) correspond to the surrounding SNR G320.4–1.2 (Whiteoak & Green 1996). TeV emission from the High Energy Stereoscopic System is shown in green (Aharonian et al., 2005b). The cross marks the position of PSR B1509-58.

The line of sight to pulsar A passes within ≈0.01 light-seconds of pulsar B, well within the unperturbed light cylinder radius of the slower pulsar. For ≈30 s at conjunction, the pulse-averaged radio emission from A is modulated with a complicated time-dependence, showing intermittent periodicities at both 50% and 100% of the rotational period of pulsar B (McLaughlin et al., 2004b). Detailed modeling shows that this behavior can be interpreted as synchrotron absorption from a relativistic plasma confined by a dipolar magnetic field, providing direct evidence for the field geometry commonly adopted in pulsar electrodynamics (Rafikov & Goldreich 2005; Lyutikov & Thompson 2005).

Drifting subpulses in the pulsed emission from pulsar B are also observed, with fluctuations at the beat frequency between the periods of A and B, and with a separation between drifting features corresponding to the period of A (McLaughlin et al., 2004a). This provides clear evidence that pulsed radiation from A is interacting with

the magnetosphere of B, supporting the conclusion that pulsar winds are magnetically dominated ($\sigma \gg 1$) in their inner regions, as discussed in Section 4.1.

Other binary systems also provide information on conditions very close to the pulsar. PSR B1957+20 is in a circular 9.2-hour orbit around a $\sim$0.025 $M_\odot$ companion, interaction with which produces a termination shock just 1.5×10^{11} cm from the pulsar[8] (Phinney et al., 1988). The X-ray flux from this nebula shows possible modulation at the orbital period (Stappers et al., 2003), as should result from Doppler boosting of the flow around the companion (Arons & Tavani 1993). PSR B1259-63 is in a highly eccentric 3.4-year orbit around a Be star. Near periastron, the pulsar is subject to a time-varying external pressure, producing a transient X-ray/radio synchrotron nebula plus TeV emission from IC scattering of light from the companion star (e.g., Johnston et al., 2005; Aharonian et al., 2005c). At future periastra of this system, coordinated X- and γ-ray observations with INTEGRAL, GLAST, and HESS can directly probe particle acceleration in this pulsar's wind (Tavani & Arons 1997; Kirk, Ball & Skjæraasen 1999).

SUMMARY POINTS

1. A magnetized relativistic wind is the main reservoir for a pulsar's rotational energy loss. The termination of this wind due to surrounding pressure produces a pulsar wind nebula (PWN), usually observed as a synchrotron nebula. A high velocity pulsar can also produce a line-emitting optical bow shock where the pulsar wind shocks surrounding gas.
2. PWNe move through a series of distinct evolutionary states, moderated by the pulsar's location (inside a supernova remnant versus in interstellar gas), the ambient conditions (cold ejecta versus shocked ejecta versus interstellar medium) and the Mach number of the pulsar (subsonic versus mildly supersonic versus highly supersonic).
3. High resolution X-ray observations of young pulsars reveal the imprint of the rotation axis on the morphology of the surrounding PWN, in the form of equatorial tori, polar jets, and overall elongation of the nebula. Using these structures, one can locate the wind termination shock and can infer the composition, flow speed, and geometry of the pulsar's wind.
4. An increasing number of bow shocks are being found around high-velocity pulsars. These systems impose a second axis of symmetry on the PWN, providing additional probes of the pulsar's wind and environment.

ACKNOWLEDGMENTS

We thank NASA for generous support through the LTSA and General Observer programs, and the Radcliffe Institute for hosting a stimulating PWN workshop in

[8]On much larger scales, PSR B1957+20 also powers a bow shock, as shown in **Figure 4*b***.

Annu. Rev. Astro. Astrophys. 2006.44:17-47. Downloaded from arjournals.annualreviews.org
by University of Bologna on 10/31/08. For personal use only.

2005. We also acknowledge support from an Alfred P. Sloan Research Fellowship (BMG) and from NASA Contract NAS8-03060 (POS). We have used images provided by Tracey DeLaney, Bruno Khélifi, CXC/SAO, NRAO/AUI, and ESO. We thank Shami Chatterjee, Roger Chevalier, Maxim Lyutikov and Steve Reynolds for useful discussions and suggestions. Finally, we thank our other enthusiastic collaborators on PWNe, most notably Jon Arons, Rino Bandiera, Fernando Camilo, Yosi Gelfand, David Helfand, Jack Hughes, Vicky Kaspi, Fred Seward, Ben Stappers, and Eric van der Swaluw.

LITERATURE CITED

Aharonian F, Akhperjanian AG, Aye KM, Bazer-Bachi AR, Beilicke M, et al. 2005a. *Astron. Astrophys.* 432:L25–29

Aharonian F, Akhperjanian AG, Aye KM, Bazer-Bachi AR, Beilicke M, et al. 2005b. *Astron. Astrophys.* 435:L17–20

Aharonian F, Akhperjanian AG, Aye KM, Bazer-Bachi AR, Beilicke M, et al. 2005c. *Astron. Astrophys.* 442:1–10

Arons J. 1983. *Nature* 302:301–5

Arons J. 2002. In *Neutron Stars in Supernova Remnants*, ed. PO Slane, BM Gaensler, pp. 71–80. San Francisco: Astronomical Society of the Pacific

Arons J, Tavani M. 1993. *Ap. J.* 403:249–55

Atoyan AM, Aharonian FA. 1996. *Astron. Astrophys. Suppl.* 120:453–56

Bandiera R. 1993. *Astron. Astrophys.* 276:648–54

Bartel N, Bietenholz MF. 2005. *Adv. Space Res.* 35:1057–64

Becker W, Trümper J. 1997. *Astron. Astrophys.* 326:682–91

Begelman MC. 1998. *Ap. J.* 493:291–300

Begelman MC, Li ZY. 1992. *Ap. J.* 397:187–95

Bell JF, Bailes M, Manchester RN, Weisberg JM, Lyne AG. 1995. *Ap. J.* 440:L81–83

Bietenholz MF, Bartel N, Rupen MP. 2004. *Science* 304:1947–49

Bietenholz MF, Hester JJ, Frail DA, Bartel N. 2004. *Ap. J.* 615:794–804

Blandford RD, Ostriker JP, Pacini F, Rees MJ. 1973. *Astron. Astrophys.* 23:145–46

Blondin JM, Chevalier RA, Frierson DM. 2001. *Ap. J.* 563:806–15

Bogovalov SV, Chechetkin VM, Koldoba AV, Ustyugova GV. 2005. *MNRAS* 358:705–14

Bogovalov SV, Khangoulyan DV. 2002. *Astron. Lett.* 28:373–85

Bucciantini N. 2002a. *Astron. Astrophys.* 387:1066–73

Bucciantini N. 2002b. *Astron. Astrophys.* 393:629–35

Bucciantini N, Amato E, Bandiera R, Blondin JM, Del Zanna L. 2004. *Astron. Astrophys.* 423:253–65

Bucciantini N, Amato E, Del Zanna L. 2005. *Astron. Astrophys.* 434:189–99

Bucciantini N, Bandiera R. 2001. *Astron. Astrophys.* 375:1032–39

Bucciantini N, Blondin JM, Del Zanna L, Amato E. 2003. *Astron. Astrophys.* 405:617–26

Camilo F, Ransom SM, Gaensler BM, Slane PO, Lorimer DR, et al. 2006. *Ap. J.* 637:456–65

Annu. Rev. Astro. Astrophys. 2006.44:17-47. Downloaded from arjournals.annualreviews.org
by University of Bologna on 10/31/08. For personal use only.

Chatterjee S, Cordes JM. 2002. *Ap. J.* 575:407–18
Chevalier RA. 1977. In *Supernovae*, ed. DN Schramm, pp. 53–61. Dordrecht: Reidel
Chevalier RA. 1998. *Mem. Soc. Astron. It.* 69:977–87
Chevalier RA. 2005. *Ap. J.* 619:839–55
Chevalier RA, Fransson C. 1992. *Ap. J.* 395:540–52
Cocke WJ, Disney MJ, Taylor DJ. 1969. *Nature* 221:525–27
Cordes JM, Romani RW, Lundgren SC. 1993. *Nature* 362:133–35
Cox DP. 1972. *Ap. J.* 178:159–68
Daugherty JK, Harding AK. 1982. *Ap. J.* 252:337–47
de Jager OC, Harding AK, Michelson PF, Nel HI, Nolan PL, et al. 1996. *Ap. J.* 457:253–66
Del Zanna L, Amato E, Bucciantini N. 2004. *Astron. Astrophys.* 421:1063–73
Dodson R, Legge D, Reynolds JE, McCulloch PM. 2003. *Ap. J.* 596:1137–41
Duncan AR, Stewart RT, Haynes RF, Jones KL. 1996. *MNRAS* 280:252–66
Frail DA, Giacani EB, Goss WM, Dubner G. 1996. *Ap. J.* 464:L165–68
Frail DA, Kassim NE, Cornwell TJ, Goss WM. 1995. *Ap. J.* 454:L129–32
Frail DA, Kulkarni SR. 1991. *Nature* 352:785–87
Frail DA, Kulkarni SR, Bloom JS. 1999. *Nature* 398:127–29
Frail DA, Scharringhausen BR. 1997. *Ap. J.* 480:364–70
Fryer CL, Colgate SA, Pinto PA. 1999. *Ap. J.* 511:885–95
Gaensler BM, Arons J, Kaspi VM, Pivovaroff MJ, Kawai N, Tamura K. 2002. *Ap. J.* 569:878–93
Gaensler BM, Jones DH, Stappers BW. 2002. *Ap. J.* 580:L137–41
Gaensler BM, Kouveliotou C, Gelfand JD, Taylor GB, Eichler D, et al. 2005. *Nature* 434:1104–6
Gaensler BM, Stappers BW, Frail DA, Moffett DA, Johnston S, Chatterjee S. 2000. *MNRAS* 318:58–66
Gaensler BM, van der Swaluw E, Camilo F, Kaspi VM, Baganoff FK, et al. 2004. *Ap. J.* 616:383–402
Gallant YA, Arons J. 1994. *Ap. J.* 435:230–60
Giacani EB, Dubner GM, Kassim NE, Frail DA, Goss WM, et al. 1997. *Ap. J.* 113:1379–90
Ginzburg VL, Syrovatskii SI. 1965. *Annu. Rev. Astron. Astrophys.* 3:297–350
Gold T. 1969. *Nature* 221:25–27
Goldreich P, Julian WH. 1969. *Ap. J.* 157:869–80
Gonzalez M, Safi-Harb S. 2003. *Ap. J.* 591:L143–46
Gotthelf EV. 2004. In *Young Neutron Stars and Their Environments*, ed. F. Camilo, BM. Gaensler, pp. 225–28. San Francisco: Astron. Soc. Pac.
Graves GJM, Challis PM, Chevalier RA, Crotts A, Filippenko AV, et al. 2005. *Ap. J.* 629:944–59
Green DA. 2004. *Bull. Astron. Soc. India* 32:335–70
Green DA, Scheuer PAG. 1992. *MNRAS* 258:833–40
Gupta Y, Mitra D, Green DA, Acharyya A. 2005. *Curr. Sci.* 89:853–56
Gvaramadze VV. 2004. *Astron. Astrophys.* 415:1073–78
Halpern JP, Gotthelf EV, Becker RH, Helfand DJ, White RL. 2005. *Ap. J.* 632:L29–32

Annu. Rev. Astro. Astrophys. 2006.44:17-47. Downloaded from arjournals.annualreviews.org
by University of Bologna on 10/31/08. For personal use only.

Harding AK, Contopoulos I, Kazanas D. 1999. *Ap. J.* 525:L125–28
Helfand DJ, Collins BF, Gotthelf EV. 2003. *Ap. J.* 582:783–92
Hester JJ, Mori K, Burrows D, Gallagher JS, Graham JR, et al. 2002. *Ap. J.* 577:L49–52
Hester JJ, Scowen PA, Sankrit R, Burrows CJ, Gallagher III JS, et al. 1995. *Ap. J.* 448:240–63
Hester JJ, Stone JM, Scowen PA, Jun B, Gallagher JS, et al. 1996. *Ap. J.* 456:225–33
Hughes JP, Slane PO, Burrows DN, Garmire G, Nousek JA, et al. 2001. *Ap. J.* 559:L153–56
Hurley K, Kouveliotou C, Cline T, Mazets E, Golenetskii S, et al. 1999. *Ap. J.* 523:L37–40
Johnston S, Ball L, Wang N, Manchester RN. 2005. *MNRAS* 358:1069–75
Jones DH, Stappers BW, Gaensler BM. 2002. *Astron. Astrophys.* 389:L1–5
Jun BI. 1998. *Ap. J.* 499:282–93
Kaspi VM, Gotthelf EV, Gaensler BM, Lyutikov M. 2001. *Ap. J.* 562:L163–66
Kaspi VM, Roberts MSE, Harding AK. 2006. In *Compact Stellar X-ray Sources*, ed. WHG Lewin, M van der Klis. Cambridge: CUP In press. **http://arxiv.org/abs/astro-ph/0402136**
Kennel CF, Coroniti FV. 1984a. *Ap. J.* 283:694–709
Kennel CF, Coroniti FV. 1984b. *Ap. J.* 283:710–30
Kirk J, Ball L, Skjæraasen O. 1999. *Astropart. Phys.* 10:31–45
Komissarov SS, Lyubarsky YE. 2004. *MNRAS* 349:779–92
Kulkarni SR, Hester JJ. 1988. *Nature* 335:801–3
Lai D. 2004. In *Cosmic Explosions in Three Dimensions: Asymmetries in Supernovae and Gamma-Ray Bursts*, ed. P Höflich, P Kumar, JC Wheeler, pp. 276–84. Cambridge: CUP
Lai D, Chernoff DF, Cordes JM. 2001. *Ap. J.* 549:1111–18
Livingstone MA, Kaspi VM, Gavriil FP. 2005. *Ap. J.* 633:1095–100
Lu FJ, Wang QD, Aschenbach B, Durouchoux P, Song LM. 2002. *Ap. J.* 568:L49–52
Lyne AG, Burgay M, Kramer M, Possenti A, Manchester RN, et al. 2004. *Science* 303:1153–57
Lyutikov M, Thompson C. 2005. *Ap. J.* 634:1223–41
Manchester RN, Hobbs GB, Teoh A, Hobbs M. 2005. *Astron. J.* 129:1993–2006
Manchester RN, Taylor JH. 1977. *Pulsars* San Francisco: Freeman
Matheson H, Safi-Harb S. 2005. *Adv. Space Res.* 35:1099–1105
McLaughlin MA, Kramer M, Lyne AG, Lorimer DR, Stairs IH, et al. 2004a. *Ap. J.* 613:L57–60
McLaughlin MA, Lyne AG, Lorimer DR, Possenti A, Manchester RN, et al. 2004b. *Ap. J.* 616:L131–34
McLaughlin MA, Stairs IH, Kaspi VM, Lorimer DR, Kramer M, et al. 2003. *Ap. J.* 591:L135–38
Melatos A. 1998. *Mem. Soc. Astron. It.* 69:1009–15
Melatos A. 2004. In *Young Neutron Stars and Their Environments*, ed. F. Camilo, BM. Gaensler, pp. 143–50. San Francisco: Astron. Soc. Pac.
Melatos A, Scheltus D, Whiting MT, Eikenberry SS, Romani RW, et al. 2005. *Ap. J.* 633:931–40

Annu. Rev. Astro. Astrophys. 2006.44:17-47. Downloaded from arjournals.annualreviews.org
by University of Bologna on 10/31/08. For personal use only.

Migliazzo JM, Gaensler BM, Backer DC, Stappers BW, van der Swaluw E, Strom RG. 2002. *Ap. J.* 567:L141–44
Minkowski R. 1942. *Ap. J.* 96:199–213
Ng CY, Romani RW. 2004. *Ap. J.* 601:479–84
Olbert CM, Clearfield CR, Williams NE, Keohane JW, Frail DA. 2001. *Ap. J.* 554:L205–8
Pacini F. 1967. *Nature* 216:567–68
Pacini F, Salvati M. 1973. *Ap. J.* 186:249–65
Pavlov GG, Teter MA, Kargaltsev O, Sanwal D. 2003. *Ap. J.* 591:1157–71
Pelling RM, Paciesas WS, Peterson LE, Makishima K, Oda M, et al. 1987. *Ap. J.* 319:416–25
Petre R, Kuntz KD, Shelton RL. 2002. *Ap. J.* 579:404–10
Phinney ES, Evans CR, Blandford RD, Kulkarni SR. 1988. *Nature* 333:832–34
Rafikov RR, Goldreich P. 2005. *Ap. J.* 631:488–94
Rees MJ, Gunn JE. 1974. *MNRAS* 167:1–12
Reynolds SP. 1988. *Ap. J.* 327:853–58
Reynolds SP. 2003. In *Cosmic Explosions: On the 10th Anniversary of SN 1993J (IAU Colloquium 192)* Suppl., ed. JM Marcaide, KW Weiler, pp. 161–65. Springer: Berlin. **http://arxiv.org/abs/astro-ph/0308483**
Reynolds SP, Aller HD. 1988. *Ap. J.* 327:845–52
Reynolds SP, Chevalier RA. 1984. *Ap. J.* 278:630–48
Reynolds SP, Fix JD. 1987. *Ap. J.* 322:673–80
Richards DW, Comella JM. 1969. *Nature* 222:551–52
Romanova MM, Chulsky GA, Lovelace RVE. 2005. *Ap. J.* 630:1020–28
Seward FD, Gorenstein P, Smith RK. 2006. *Ap. J.* 636:873–80
Shakeshaft JR. 1979. *Astron. Astrophys.* 72:L9
Shull JM, Fesen RA, Saken JM. 1989. *Ap. J.* 346:860–68
Slane P, Chen Y, Schulz NS, Seward FD, Hughes JP, Gaensler BM. 2000. *Ap. J.* 533:L29–32
Slane P, Helfand DJ, van der Swaluw E, Murray SS. 2004. *Ap. J.* 616:403–13
Slane PO, Helfand DJ, Murray SS. 2002. *Ap. J.* 571:L45–49
Spitkovsky A, Arons J. 2004. *Ap. J.* 603:669–81
Staelin DH, Reifenstein EC III. 1968. *Science* 162:1481–83
Stappers BW, Gaensler BM, Kaspi VM, van der Klis M, Lewin WHG. 2003. *Science* 299:1372–74
Stephenson FR, Green DA. 2002. *Historical Supernovae and Their Remnants*. Oxford: Oxford University
Tavani M, Arons J. 1997. *Ap. J.* 477:439–64
Thompson C, Duncan RC, Woods PM, Kouveliotou C, Finger MH, van Paradijs J. 2000. *Ap. J.* 543:340–50
Thompson C, Lyutikov M, Kulkarni SR. 2002. *Ap. J.* 574:332–55
Trimble V. 1982. *Rev. Mod. Phys.* 54:1183–1224
Truelove JK, McKee CF. 1999. *Ap. J. Suppl.* 120:299–326
Trussoni E, Massaglia S, Caucino S, Brinkmann W, Aschenbach B. 1996. *Astron. Astrophys.* 306:581–86

Annu. Rev. Astro. Astrophys. 2006.44:17-47. Downloaded from arjournals.annualreviews.org
by University of Bologna on 10/31/08. For personal use only.

van den Bergh S. 1978. *Ap. J.* 220:L9–10
van der Swaluw E. 2003. *Astron. Astrophys.* 404:939–47
van der Swaluw E, Achterberg A, Gallant YA. 1998. *Mem. Soc. Astron. It.* 69:1017–22
van der Swaluw E, Achterberg A, Gallant YA. 2002. In *Neutron Stars in Supernova Remnants*, ed. PO Slane, BM Gaensler, pp. 135–40. San Francisco: Astron. Soc. Pac.
van der Swaluw E, Achterberg A, Gallant YA, Downes TP, Keppens R. 2003. *Astron. Astrophys.* 397:913–20
van der Swaluw E, Achterberg A, Gallant YA, Tóth G. 2001. *Astron. Astrophys.* 380:309–17
van der Swaluw E, Downes TP, Keegan R. 2004. *Astron. Astrophys.* 420:937–44
van Kerkwijk MH, Kulkarni SR. 2001. *Astron. Astrophys.* 380:221–37
Wang QD, Li ZY, Begelman MC. 1993. *Nature* 364:127–29
Weekes TC, Cawley MF, Fegan DJ, Gibbs KG, Hillas AM, et al. 1989. *Ap. J.* 342:379–95
Weiler KW, Panagia N. 1978. *Astron. Astrophys.* 70:419–22
Weisskopf MC, Hester JJ, Tennant AF, Elsner RF, Schulz NS, et al. 2000. *Ap. J.* 536:L81–84
Whiteoak JBZ, Green AJ. 1996. *Astron. Astrophys. Suppl.* 118:329–43
Wilkin FP. 1996. *Ap. J.* 459:L31–34
Wilkin FP. 2000. *Ap. J.* 532:400–14
Willingale R, Aschenbach B, Griffiths RG, Sembay S, Warwick RS, et al. 2001. *Astron. Astrophys.* 365:L212–17
Woltjer L, Salvati M, Pacini F, Bandiera R. 1997. *Astron. Astrophys.* 325:295–99
Woods PM, Kouveliotou C, Göğüş E, Finger MH, Swank J, et al. 2002. *Ap. J.* 576:381–90
Woods PM, Thompson C. 2006. In *Compact Stellar X-ray Sources*, ed. WHG Lewin, M van der Klis. Cambridge: CUP In press. **http://arxiv.org/abs/astro-ph/0406133**
Yusef-Zadeh F, Bally J. 1987. *Nature* 330:455–58

RELATED RESOURCES

Davidson K, Fesen RA. 1985. *Annu. Rev. Astron. Astrophys.* 23:119–46
Weiler KW, Sramek RA. 1988. *Annu. Rev. Astron. Astrophys.* 26:295–341
Woltjer L. 1972. *Annu. Rev. Astron. Astrophys.* 10:129:58
Internet supernova remnant catalog: **http://www.mrao.cam.ac.uk/surveys/snrs/**
Internet pulsar catalog: **http://www.atnf.csiro.au/research/pulsar/psrcat/**
Internet pulsar wind nebula catalog: **http://www.physics.mcgill.ca/∼pulsar/pwncat.html**

Annu. Rev. Astro. Astrophys. 2006.44:17-47. Downloaded from arjournals.annualreviews.org
by University of Bologna on 10/31/08. For personal use only.

Annual Review
of Astronomy
and Astrophysics

Volume 44, 2006

Contents

An Engineer Becomes an Astronomer
Bernard Mills 1

The Evolution and Structure of Pulsar Wind Nebulae
Bryan M. Gaensler and Patrick O. Slane 17

X-Ray Properties of Black-Hole Binaries
Ronald A. Remillard and Jeffrey E. McClintock 49

Absolute Magnitude Calibrations of Population I and II Cepheids and Other Pulsating Variables in the Instability Strip of the Hertzsprung-Russell Diagram
Allan Sandage and Gustav A. Tammann 93

Stellar Population Diagnostics of Elliptical Galaxy Formation
Alvio Renzini 141

Extragalactic Globular Clusters and Galaxy Formation
Jean P. Brodie and Jay Strader 193

First Fruits of the *Spitzer Space Telescope*: Galactic and Solar System Studies
Michael Werner, Giovanni Fazio, George Rieke, Thomas L. Roellig, and Dan M. Watson 269

Populations of X-Ray Sources in Galaxies
G. Fabbiano 323

Diffuse Atomic and Molecular Clouds
Theodore P. Snow and Benjamin J. McCall 367

Observational Constraints on Cosmic Reionization
Xiaohui Fan, C.L. Carilli, and B. Keating 415

X-Ray Emission from Extragalactic Jets
D.E. Harris and Henric Krawczynski 463

The Supernova–Gamma-Ray Burst Connection
S.E. Woosley and J.S. Bloom 507

Annu. Rev. Astro. Astrophys. 2006.44:17-47. Downloaded from arjournals.annualreviews.org
by University of Bologna on 10/31/08. For personal use only.

Indexes

Subject Index 557

Cumulative Index of Contributing Authors, Volumes 33–44 567

Cumulative Index of Chapter Titles, Volumes 33–44 570

Errata

An online log of corrections to *Annual Review of Astronomy and Astrophysics* chapters (if any, 1997 to the present) may be found at http://astro.annualreviews.org/errata.shtml

Annu. Rev. Astro. Astrophys. 2006.44:17-47. Downloaded from arjournals.annualreviews.org
by University of Bologna on 10/31/08. For personal use only.